J Physiol 589.9 (2011) pp 2321–2348

The Journal of Physiology

Ectopic expression of cone-specific G-protein-coupled receptor kinase GRK7 in zebrafish rods leads to lower photosensitivity and altered responses

F. Vogalis[1,2], T. Shiraki[3], D. Kojima[3], Y. Wada[3], Y. Nishiwaki[4], J. L. P. Jarvinen[1,2,5], J. Sugiyama[3], K. Kawakami[6,7], I. Masai[4], S. Kawamura[8,9], Y. Fukada[3] and T. D. Lamb[1,2]

[1]*Department of Neuroscience, John Curtin School of Medical Research, and* [2]*ARC Centre of Excellence in Vision Science, Australian National University, Canberra, ACT 0200, Australia*

[3]*Department of Biophysics and Biochemistry, Graduate School of Science, University of Tokyo, Hongo 7-3-1, Bunkyo-Ku, Tokyo 113-0033, Japan*

[4]*Developmental Neurobiology Unit, Okinawa Institute of Science and Technology Promotion Corporation (OIST), 1919-1 Azatancha, Onna, Okinawa 904-0412, Japan*

[5]*Faculty of Life and Social Sciences, Swinburne University of Technology, Hawthorn, VIC 3122, Australia*

[6]*Division of Molecular and Developmental Biology, National Institute of Genetics and* [7]*Department of Genetics, Graduate University for Advanced Studies (SOKENDAI), Mishima, Shizuoka 411-8540, Japan*

[8]*Graduate School of Frontier Biosciences and* [9]*Department of Biology, Graduate School of Science, Osaka University, Suita, Osaka 565-0871, Japan*

Non-technical summary When rod and cone photoreceptors in the eye respond to light, they need to recover, and the first step in recovery involves a protein called G-protein receptor kinase (GRK). Rods, which underlie night vision, employ a variant called GRK1, whereas cones, which mediate day vision, typically employ a variant called GRK7. We have engineered rod cells in the zebrafish retina that additionally express the cone variant, GRK7. By recording electrically from these modified rods, we have found that they are less sensitive to light than normal rods, in that regard mimicking cones. We have also found evidence to suggest that the size of the cell's response to a single photon (the smallest particle of light) is normal when recovery is mediated by GRK1, but is small (and hence somewhat cone-like) when mediated by GRK7. These results help us understand the differences between rod and cone photoreceptors.

Abstract To investigate the roles of G-protein receptor kinases (GRKs) in the light responses of vertebrate photoreceptors, we generated transgenic zebrafish lines, the rods of which express either cone GRK (GRK7) or rod GRK (GRK1) in addition to the endogenous GRK1, and we then measured the electrophysiological characteristics of single-cell responses and the behavioural responses of intact animals. Our study establishes the zebrafish expression system as a convenient platform for the investigation of specific components of the phototransduction cascade. The addition of GRK1 led to minor changes in rod responses. However, exogenous GRK7 in GRK7-tg animals led to lowered rod sensitivity, as occurs in cones, but surprisingly to slower response kinetics. Examination of responses to long series of very dim flashes suggested the possibility that the GRK7-tg rods generated two classes of single-photon response, perhaps corresponding to the interaction of activated rhodopsin with GRK1 (giving a standard response) or with GRK7 (giving a very small response). Behavioural measurement of optokinetic responses (OKR) in intact GRK7-tg zebrafish larvae showed that the overall rod visual pathway was less sensitive, in accord with the lowered sensitivity of the rods. These results help provide an understanding for the molecular basis of the electrophysiological differences between cones and rods.

F. Vogalis, T. Shiraki and D. Kojima contributed equally to this work.

DOI: 10.1113/jphysiol.2010.204156

(Received 15 December 2010; accepted after revision 2 March 2011; first published online 8 March 2011)
Corresponding authors T. D. Lamb: Department of Neuroscience, John Curtin School of Medical Research, and ARC Centre of Excellence in Vision Science, Australian National University, Canberra, ACT 0200, Australia. Email: trevor.lamb@anu.edu.au; and Y. Fukada: Department of Biophysics and Biochemistry, Graduate School of Science, University of Tokyo, Hongo 7-3-1, Bunkyo-Ku, Tokyo 113-0033, Japan. Email: sfukada@mail.ecc.u-tokyo.ac.jp

Abbreviations CCW, counter-clockwise; CW, clockwise; dpf, days post-fertilization; GC, guanylate cyclase; GCAP, guanylate cyclase activating protein; GPCR, G-protein coupled receptor; GRK, G-protein coupled receptor kinase; Gtα, G-protein transducin α-subunit; OKR, optokinetic response; PDE, phosphodiesterase; RGS, regulator of G-protein signalling; -tg, transgenic; WT, wild-type.

Introduction

The rod and cone photoreceptors of the vertebrate retina exhibit many similarities but also key differences. Cones have fast response kinetics and they function over an enormous range of light intensities, from twilight levels upwards; importantly, cones can avoid saturation no matter how bright the intensity of steady illumination becomes. Rods, on the other hand, are specialized for operation at extremely low levels of illumination, and can reliably detect individual photons of light. Their responses are slower, and their flash sensitivity about an order of magnitude higher, than for cones.

Apart from topological differences in outer segment membrane organization, cones and rods exhibit qualitative and quantitative differences in the proteins of phototransduction. The overall cascade of reactions is closely similar, but some proteins are expressed as distinct isoforms between cones and rods, e.g. transducin α-subunit as Gt2α in cones but Gt1α in rods (Hurley, 1992; Hisatomi & Tokunaga, 2002; Fu & Yau, 2007; Kawamura & Tachibanaki, 2008). In addition, substantial differences between cones and rods exist in the expression levels of some of the proteins. Accordingly, it is possible that many of the differences in physiological response properties arise from differences in the activities and/or expression levels of the transduction proteins.

In this study, we have examined the role of retinal G-protein-coupled receptor kinases (GRKs) in rods of the zebrafish (*Danio rerio*), a species that has a relatively high proportion of cones. GRKs phosphorylate the activated G-protein-coupled receptor (GPCR) near its C-terminus, enabling the capping protein arrestin to bind and thereby shut-off the activity of the activated GPCR (Maeda *et al.* 2003). GRK1, or rhodopsin kinase, is the GRK isoform expressed in all rods. The GRK isoform expressed in cones differs amongst vertebrate species; cones in some species express GRK1 at a higher level than in rods (Zhao *et al.* 1998), whereas cones in many other species including teleosts express GRK7 (Hisatomi *et al.* 1998). In fact, knockdown of GRK7–1 in larval zebrafish impairs cone response recovery (Rinner *et al.* 2005), suggesting an essential role for GRK7 in cones.

Our recent studies (Tachibanaki *et al.* 2001, 2005; Wada *et al.* 2006) have examined GRKs and phosphorylation in teleost photoreceptors, and have shown: (1) that phosphorylation of activated visual pigment is much faster in cones than in rods; (2) that GRK7 exhibits much higher enzymatic activity than does GRK1; and (3) that the expression level of GRK7 in cones is much higher than that of GRK1 in rods.

These findings suggest that the combination of the difference in kinase activity and the difference in expression level between GRK1 in rods and GRK7 in cones contribute to the difference in the photoresponse properties of the cells. To examine this hypothesis, we generated transgenic zebrafish ectopically expressing GRK7–1 in their rods (GRK7-tg), and measured the expression level of the relevant proteins in the rods. We characterized the electrical responses of individual rod photoreceptors and examined rod-mediated behaviour in intact animals. Our results reveal the functional changes consequent upon exogenous expression of GRK7 in rods, and help provide an understanding of the molecular basis for the electrophysiological differences between cones and rods.

Methods

Ethical approval

Ethical approval for the experiments was granted by the Animal Experimentation Ethics Committee of the Australian National University, and the work conformed to the provisions of the Australian Code of Practice for the Care and Use of Animals for Scientific Purposes and to the principles of UK regulations.

Generation of zebrafish expressing GRK1 and GRK7 transgenes in rod photoreceptors

Fish were treated in accordance with the guidelines of the University of Tokyo. The wild-type zebrafish strain RIKEN WT was originally a gift from Dr Hitoshi Okamoto (Brain Science Institute, Riken) and bred in the Tokyo

laboratory. They were maintained on 14 h light–10 h dark cycles, and fed twice per day with living baby brine shrimp. We generated transgenic zebrafish that over-express GRK7–1 or GRK1A (Wada *et al.* 2006) in rods under the control of the zebrafish rhodopsin promoter (Asaoka *et al.* 2002) by using the *Tol2*-based transgenesis system (Kawakami *et al.* 2004) as follows. A DNA fragment which contains the rhodopsin promoter followed by the GRK7–1 or GRK1A open reading frame was subcloned into pT2KXIGΔin (Urasaki *et al.* 2006) by replacing the pre-existing EF1α promoter and GFP open reading frame via a double digestion with *Xho*I and *Bgl*II followed by ligation. The resulting transgene construct is shown in Fig. 1*A*. The *Tol2* transposase mRNA was transcribed from pCS-TP (Kawakami *et al.* 2004) *in vitro* using the mCAP mRNA Capping Kit (Stratagene, La Jolla, CA, USA) or the mMESSAGE mMACHINE kit (Ambion, Inc., Austin, TX, USA). About 1 nl of DNA/RNA solution containing 25 ng μl^{-1} DNA of the transgene construct and 5 ng μl^{-1} *Tol2* mRNA in 0.1 M KCl/0.05% phenol red was injected into wild-type embryos at the one-cell stage. F_0 founder fish were identified by PCR analysis of the genomic DNA pools of their F_1 embryos with a pair of primers, SV40-polyA-Fw (5′-GCGAC TCTAG ATCAT AATCA GCC-3′) and Tol2-Rv (5′-AGTCC AAAAT CAGCC ACAGG-3′), which were designed to amplify a 299 bp DNA fragment. We established three transgenic lines for GRK7 and two transgenic lines for GRK1. These transgenic lines had a single copy of the transgene at distinct integration sites in the genome, as confirmed by Southern blot analysis as follows. Briefly, a digoxigenin-labelled DNA probe for the zebrafish rhodopsin promoter was prepared from the Rh(–1084) plasmid (Asaoka *et al.* 2002) by using PCR DIG Probe Synthesis Kit (Roche Diagnostics GmbH, Mannheim, Germany) with a pair of primers (5′-GAATG AATAA ATGTT CCAAA GCAG-3′ and 5′-TTCCA TGATC AAGAC TCAGA AGG-3′). Genomic DNA prepared from the fish fin was digested with *Eco*RV, electrophoresed on 0.7% agarose gel, and transferred to a nylon membrane (Hybond-N+, GE Healthcare) by capillary blotting with 0.4 M NaOH. The membrane was incubated with the DNA probe at 55°C in a hybridization buffer composed of 50% formamide, 5 × SSC (1 × SSC contains 0.15 M NaCl and 0.015 M sodium citrate), 0.1% *N*-lauroylsarcosine sodium salt, 0.02% SDS and 2% blocking reagent (Roche Diagnostics GmbH, Mannheim, Germany). Hybridization signals were detected by using DIG Luminescent Detection Kit (Roche Diagnostics GmbH, Mannheim, Germany). Transgenic fish were maintained as hemizygotes, which were used in the following experiments unless otherwise stated.

Fish used for studies of the optokinetic response (OKR) were generated by breeding homozygous larvae that harboured the *eclipse* mutation (*els*) causing cone degeneration, into the GRK7-transgenic lines to eliminate cone function. At 4–5 days post-fertilization (dpf), heterozygous (*els*/+) or wild-type larvae reliably show OKR in bright light, while homozygous (*els*/*els*) larvae do not respond in the same conditions (Nishiwaki *et al.* 2008). Using this criterion, homozygous *els* carriers were selected from larvae generated from crosses between *els*/+ and *els*/+;*Tg(rho:GRK7)* fish, and were used for the OKR measurement at 21 dpf. After the OKR measurements, each larva was subjected to PCR-mediated genotyping as described above, and identified as transgenic (*els*/*els*;*Tg(rho:GRK7)*) or non-transgenic (*els*/*els*).

Immunohistochemistry

Immunohistochemistry was conducted as described previously (Wada *et al.* 2006). Eyes were isolated from light-adapted zebrafish, and 10 μm thick frozen ocular sections were prepared. These sections were incubated for 30 min at room temperature in a blocking solution composed of 0.1% Triton X-100 and 1.5% normal goat serum in phosphate-buffered saline (PBS; 15 mM Na-phosphate, 140 mM NaCl, pH 7.4), and then incubated with anti-GRK7 rabbit polyclonal antibody (1:500 dilution) raised against a partial sequence of carp GRK7 (Tachibanaki *et al.* 2005) for 24 h at 4°C. The sections were washed with PBS and incubated for 24 h at 4°C with anti-rabbit IgG antibody (Cell Signaling Technology, Inc., Danvers, MA, USA) conjugated with horseradish peroxidase. Positive signals were visualized by using a Vectastain Elite ABC kit (Vector Laboratories, Inc., Burlingame, CA, USA) with a substrate solution of 0.4 mg ml^{-1} diaminobenzidine and 0.003% H_2O_2 in 50 mM Tris-HCl (pH 7.5).

Spectrophotometric measurement of rhodopsin in transgenic eyes

Spectrophotometric measurements were performed as previously described with some modifications (Wada *et al.* 2006). Both eyes were isolated from a dark-adapted zebrafish, homogenized in 400 μl of buffer P (50 mM Hepes, 140 mM NaCl, 1 mM DTT, 10 μg ml^{-1} leupeptin, 10 μg ml^{-1} aprotinin, pH 6.6) on ice, and then centrifuged at 18,000 *g* for 30 min at 4°C. The precipitate was washed with 400 μl of buffer P, then extracted with 400 μl of buffer P containing 2% (w/v) CHAPS and centrifuged at 18,000 *g* for 30 min at 4°C. The extract was incubated at 25°C in the presence of 100 mM hydroxylamine for 1 h in order to convert essentially all of the cone visual pigment into opsin plus retinal oxime in the dark. The rhodopsin content was then estimated from the difference absorption spectrum measured before and after complete bleaching ($\lambda > 524$ nm), with the molar extinction coefficient of

rhodopsin taken to be 40,600 M^{-1} cm^{-1} as for bovine rhodopsin (Wald & Brown, 1953). As the eye size varied between individuals, the rhodopsin content was normalized by the total protein concentration of the membrane extract.

Immunoblot analysis

For immunoblot analysis, eyes or retinas were dissected from adult zebrafish (>6 months old) and homogenized in an SDS-PAGE sampling buffer (10 mM Tris-HCl, 6% glycerol, 2% SDS, 50 mM dithiothreitol, 2 mM EDTA and 0.02% Coomassie Brilliant Blue R-250, pH 6.8). The protein content of the homogenate was determined according to Bradford (1976). Proteins in the tissue homogenates were separated on an sodium dodecyl sulfate–polyacrylamide gel electrophoresis (SDS-PAGE) and were transferred to a polyvinylidene difluoride membrane (Millipore). The blotted membrane was pre-incubated with 1% (w/v) skim milk (BD Diagnostic Systems, Sparks, MD, USA) in TBS (50 mM Tris-HCl, 200 mM NaCl, 1 mM $MgCl_2$, pH7.4) for 1 h at 37°C for blocking. The membrane was then incubated with one of the following primary antibodies in the blocking solution overnight at 4°C: anti-carp GRK7 antibody, 1:1000 dilution (Tachibanaki *et al.* 2005); anti-GRK1 antibody (0.2 $\mu g\,ml^{-1}$; sc-8004, Santa Cruz Biotechnology, Inc., Santa Cruz, CA, USA); anti-GNAT1 antibody (0.2 $\mu g\,ml^{-1}$; sc-389, Santa Cruz Biotechnology); anti-carp Arr1 antiserum, 1:2000; anti-carp GC-R1 antiserum,1:400 (Takemoto *et al.* 2009); anti-frog S-modulin antiserum, 1:400 (Arinobu *et al.* 2010); or anti-carp RGS9 antiserum, 1:400 (S. Tachibanaki, S. Yonetsu, S. Fukaya & S. Kawamura, unpublished observations). The bound primary antibodies were detected by horseradish peroxidase-conjugated secondary antibodies (0.2 $\mu g\,ml^{-1}$, KPL Inc., Gaithersburg, MD, USA) in combination with an enhanced chemiluminescence detection system (Western Lightning Chemiluminescence Reagent, PerkinElmer Life Sciences). The immuno-positive signal intensities were quantified by Image Gauge software (Fujifilm).

Rhodopsin phosphorylation in retinal homogenates

Retinas were homogenized on ice with an extraction buffer (20 mM Hepes, 5 mM $MgCl_2$, 120 mM KCl, 1 mM EGTA, 1 mM DTT, 100 μM PMSF, 50 $\mu g\,ml^{-1}$ leupeptin, 50 $\mu g\,ml^{-1}$ aprotinin, pH 7.4). An aliquot of the homogenate was subjected to rhodopsin extraction with the extraction buffer containing 1% (w/v) CHAPS, and subsequently to a photo-bleaching measurement where the amount of rhodopsin was determined spectrophotometrically. The phosphorylation assay was performed in 50 μl of a reaction mixture in which the retinal homogenate was diluted with the extraction buffer to contain 0.8 μM rhodopsin. In the first step of the assay, the reaction mixture was irradiated on ice for 1 min with an intense white light (5000 lux), which completely activated rhodopsin. After irradiation, the mixture was kept at 25°C for 1 min so that the light-activated cone pigments could completely decay. Then, for initiation of the phosphorylation reaction, [γ-^{32}P]ATP was added to the mixture at 25°C, to a final concentration of 100 μM (3.7 kBq μl^{-1}). The reaction in 10 μl aliquots was terminated at various time points by mixing with 30 μl of 1.3× SDS-PAGE sampling buffer. After SDS-PAGE, the gel was subjected to autoradiography, where phosphorylation levels of light-activated rhodopsin were estimated from the band intensities.

Electrophysiological recordings from zebrafish rods

Suction pipette recordings from isolated zebrafish rods were made in the Canberra laboratory using the methods of Baylor *et al.* (1979*a*), Lamb *et al.* (1981, 1986), and Murnick & Lamb (1996). The perfusion solution was Hepes–bicarbonate buffered physiological saline of the following composition (in mM): NaCl, 112.5; KCl, 3.6; $MgCl_2$, 2.4; $CaCl_2$, 1.2; EDTA, 0.02; Hepes, 10; $NaHCO_3$, 20; D-glucose, 10; sodium glutamate, 0.5; sodium succinate, 3; its pH was adjusted to 7.40–7.45 with ∼80 μl of 1 M HCl per 200 ml. The solution was bubbled with 95% O_2–5% CO_2, and was perfused through the recording chamber at ∼0.5 ml min^{-1}. We found this solution to be better at maintaining the viability of zebrafish rods than toad Ringer solution. Suction pipettes were drawn from borosilicate glass capillary tubing (Clark GC150–10, SDR, Sydney, Australia) on a Sutter P97 puller, to have a lumen diameter of ∼2.5–3 μm after fire polishing, and were silanized as described by Jarvinen & Lamb (2005). In most experiments the suction pipette was filled with the same pre-oxygenated Hepes–bicarbonate buffered perfusion solution; the pipette resistance was 2.5–3 MΩ.

Zebrafish were maintained at 25–28°C on a 12 h light–12 h dark cycle, and fed tropical fish food; they were ∼3 cm in length when used. An individual fish was dark-adapted overnight in a light-proof tank, and then killed under dim red light by cranial concussion followed by decapitation, according to guidelines approved by the Animal Experimentation Ethics Committee of the Australian National University. All subsequent procedures were performed under infra-red illumination. The eyes were removed and placed in ice-cold L-15 medium (Gibco, USA) with added BSA (1 mg ml^{-1}) and glucose (10 mM). Under a dissecting microscope, one eye was opened by nicking the cornea with a pair of fine forceps and then the lens was removed with vitreous, retina and retinal pigment

epithelium attached. The retinal pigment epithelium readily separated from the retina, which was carefully peeled away from the lens, laid out flat on the bottom of the Petri dish with the photoreceptor layer uppermost and dissected as needed into small pieces (∼0.5 mm square) with a fine microsurgical blade (Surgistar, Knoxville, TN, USA).

A suspension of retinal material was transferred to the recording chamber on the stage of a motorized inverted microscope (Axiovert 200M, Carl Zeiss, Germany), and the pieces were allowed to settle for ∼5 min before perfusion began. Cells were visualized using an IR-sensitive CCD camera (Watec 902H) and video monitor, under IR illumination from an 850 nm LED in the modified microscope illuminator; images were recorded to a DVD recorder for later analysis. The outer segment of a single rod was drawn into the suction pipette, using a 'semi-open' suction system as described by Koskelainen *et al.* (1994); the pipette resistance increased to 5–10 MΩ. Pipette current was recorded with an A-M Systems 2400 patch clamp amplifier (modified for fine control of DC offset; A-M Systems Inc., Carlsborg, WA, USA), and was low-pass filtered at 20 Hz (8-pole Bessel, Kemo Ltd, Beckenham, UK), and digitized at either 100 or 200 Hz via custom software running under Matlab (The Mathworks, Natick, MA, USA). Experiments were performed at room temperature (22–24°C). A recording from a single zebrafish rod typically lasted 20–30 min.

Visible light stimuli were generated using a green LED (516 nm, in a second modified illuminator housing) driven by custom-designed pulse number electronics. Every 1.4 ms, the LED current could be activated for a selected number (0–16 000) of pulses from a master clock running at 12 MHz. Hence, the flash was typically 1.4 ms in duration, whereas 'steady' light was modulated at ∼700 Hz. The stimulated area was usually 38 μm in diameter, covering the outer segment. The light intensity was measured at the end of each experiment with a calibrated power meter (UDT Model 371), and flash intensities have been converted to photon μm^{-2}.

For the responses to each flash, the baseline current was taken as the mean over the 1 s interval prior to the flash. Often the baseline current drifted slowly at an approximately steady rate (typically ∼0.2 pA s^{-1}), in which case the average drift was removed from the individual traces by subtracting out the long-term slope determined from a least-squares fit to the set of baseline current measurements. The rod's maximal response was measured with a just-saturating flash presented at regular intervals, and where practicable the circulating current at intervening times was corrected by linear interpolation. Rods for which the saturating response decreased by >30% over the course of the recording were excluded from analysis. Analysis of digitized recordings was performed with Matlab, SigmaPlot (Systat Software Inc., San Jose, CA, USA) and Igor Pro 4 (WaveMetrics, Inc., Lake Oswego, OR, USA) software.

For comparison with the illumination protocols used in the whole-animal OKR studies (see below), rods were also stimulated with square-wave illumination comprising 10 cycles at 0.5 Hz (i.e. 1 s on, and 1 s off) at a range of intensities. Spectral analysis of the recordings was then used to determine the amplitude of the frequency component at 0.5 Hz, as follows. Records of 20.48 s duration (4096 samples at 200 Hz) beginning at the stimulus onset, were processed using the fast Fourier transform algorithm in Igor Pro 4, after filtering with a Hanning window, and the amplitude of the component at 0.5062 Hz was taken. To average across rods, the amplitudes were first normalized to the largest amplitude obtained at different intensities for each rod; the normalized values were then averaged across the two groups of rod (WT and GRK7-tg).

Optokinetic response measurement

The optokinetic responses (OKR) of fish were measured in the Tokyo and Okinawa laboratories according to the literature (Brockerhoff *et al.* 1995; Nishiwaki *et al.* 2008). A zebrafish larva (21 dpf) was surrounded by fine needles for mild immobilization on a 5 mm-thick clear silicone rubber fit in a 35-mm Petri dish; this suppressed whole-body movements. The larva was dark-adapted for 3–5 h at 27–30°C before measurement of the OKR. The following procedures were performed in darkness or under infrared light. The dark-adapted larva in the dish was placed at the centre of a microscope stage to which a circular drum was mounted. The drum had 18 deg wide black and white vertical stripes on the inside (i.e. 10 pairs of stripes per revolution), and was rotated by a belt linked to an adjacent motor. White light from a halogen lamp was used to illuminate the drum with neutral density filters to control the light intensity. In each OKR trial, the drum was rotated in both directions, clockwise (CW) and counter-clockwise (CCW), in the manner shown in Fig. 9*A*. In a single set of trials, we measured the OKR of the larva at two different speeds of rotation under six different light intensities. The rotational speeds were 1.5 and 3.0 revolutions per minute (rpm), corresponding respectively to angular speeds of 9 deg s^{-1} and 18 deg s^{-1}, or to square-wave illumination at any fixed point on the retina at 0.25 Hz and 0.5 Hz. The light intensities used were −4.0, −2.9, −2.6, −2.0, −0.9 and 0 (in log unit, relative to the brightest intensity, 1100 lux). The head of the larva (top view) was imaged by using an IR-sensitive video camera (C2400-79 or C2741-79; Hamamatsu Photonics) attached to a binocular microscope (Zeiss), and the larva was illuminated with IR light from below. Image sequences were digitized with an A/D converter (ADVC-55; Canopus) and recorded as digital video movies in DV-NTSC format (29.7 frame s^{-1}).

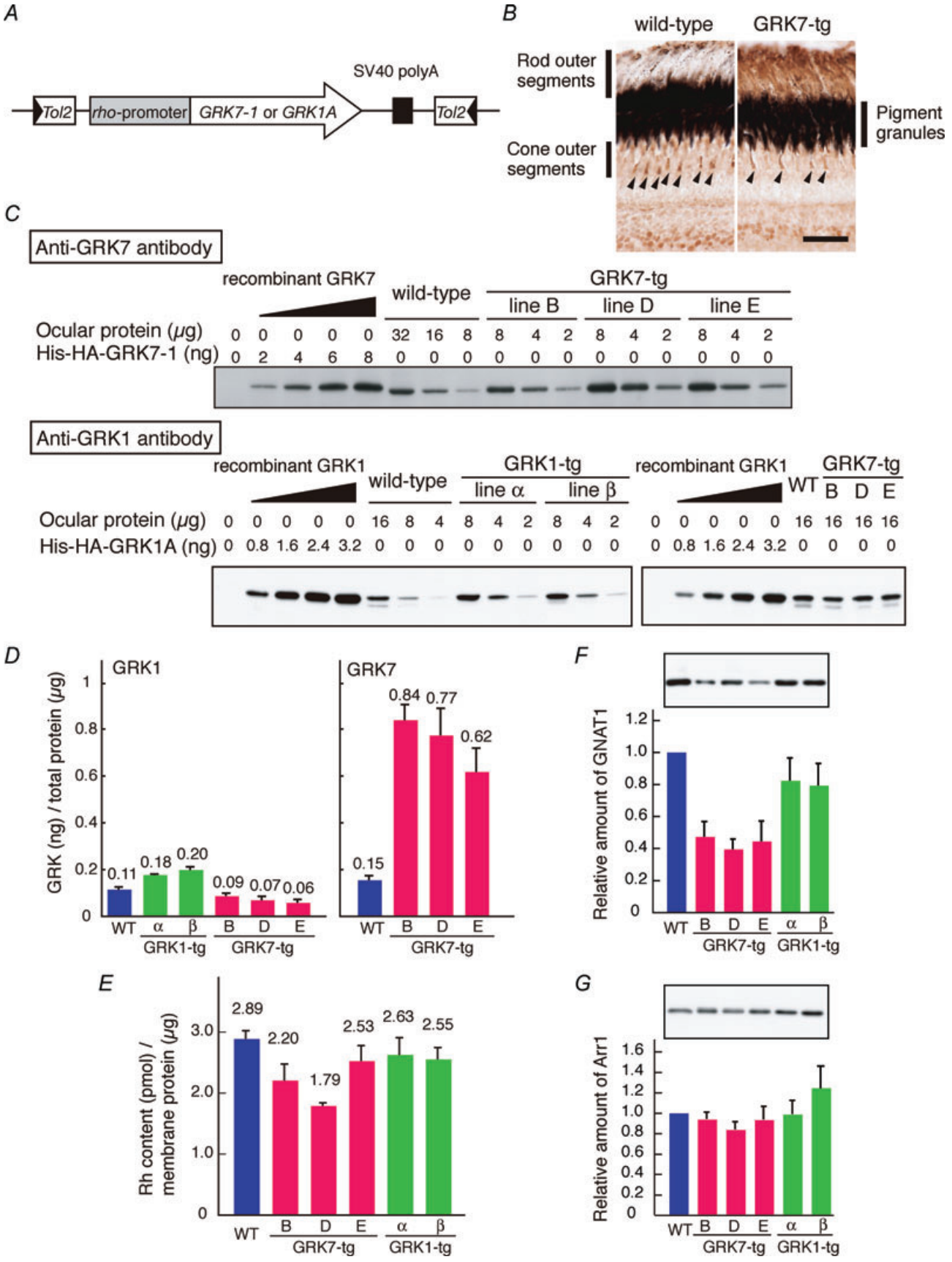

To determine whether or not the larva showed OKR in a given trial, the image sequence data were processed as follows. The infrared image sequence was converted to a .MOV file (3 frame s^{-1}) using iMovie software (Apple); sample movies (10 frame s^{-1}) are included in online Supplemental Material. The resulting .MOV file was analysed using ImageJ software (http://rsb.info.nih.gov/ij/). In each frame, the orientation of each eye was determined by fitting an ellipse to the eye shape and plotted as a function of time (Fig. 9*A*). Note that the OKR of the zebrafish larva to these rotational stimuli typically consisted of repetitions of smooth-pursuit eye movements interspersed with rapid saccades in the opposite direction. The saccadic eye movements (asterisks in Fig. 9*A*) were identified using operator-determined thresholds of the eye movement acceleration (typically 5 deg s^{-2}), and were excluded in the calculation of eye velocity. The processed data were used to calculate the mean eye velocities during each trial for the periods of CW, CCW and zero rotation; these mean eye velocities are denoted: v(CW), v(CCW) and v(ZERO). A given trial was defined as exhibiting OKR when both of the following criteria were met: (i) the mean velocities in the three conditions fulfilled the requirement v(CW) > v(ZERO) > v(CCW); and (ii) the differences between v(CW) and v(ZERO) and between v(ZERO) and v(CCW) were both statistically significant according to Student's *t* test ($P < 0.05$).

The relationship between the eye velocity and the light intensity was analysed as follows. The mean eye velocities v(CW) and v(CCW) were calculated for each eye and in each trial as described above. For each direction (CW or CCW) at each intensity, the larger absolute value of the two mean eye velocities obtained from the left and right eyes was defined as the mean velocity for CW and CCW, respectively. The highest velocity among all the conditions was defined as the maximum velocity. The mean eye velocities were then normalized to the maximum velocity for each larva. The eye velocities of larvae that did not show OKR were set to zero.

Results

Using the *Tol2*-based transgenesis system (Fig. 1*A*), we generated three GRK7-transgenic lines (GRK7B, GRK7D and GRK7E) ectopically expressing the cone-specific kinase GRK7–1 in rods, and, primarily for control purposes, two GRK1-transgenic lines (GRK1α and GRK1β) over-expressing GRK1A in rods. Throughout this paper, we will employ the terms WT, GRK7-tg, and GRK1-tg to refer respectively to wild-type zebrafish, to zebrafish with rods expressing GRK7, and to zebrafish with rods over-expressing GRK1. As a visual aid for distinguishing the strains, we employ colour-coding of traces and bars as follows: WT, blue; GRK1-tg, green; GRK7-tg, red. Note that, to minimize colour confusion for red/green anomalous readers, the red has deliberately been tinted closer to magenta.

All animals in the established lines were healthy and developed normally to adulthood. The length (*L*)

Figure 1. Expression of GRKs in transgenic zebrafish rods
A, schematic diagram of the transgene introduced into the GRK7- or GRK1-tg lines. *B*, retinal sections of adult wild-type and GRK7-tg fish were immunostained with anti-carp GRK7 antibody; scale bar, 20 μm. *C* and *D*, expression levels of GRK7 in GRK7-tg eyes, and of GRK1 in GRK7-tg and GRK1-tg eyes, were assessed by immunoblot analysis of serial dilutions of ocular homogenates from age-matched wild-type and transgenic zebrafish. The amount of protein loaded onto each lane is indicated. His-HA-tagged recombinant GRK proteins, His-HA-GRK7–1 and His-HA-GRK1A, (Wada et al. 2006), were used as standards for the calibration of ocular GRK protein levels. The ocular homogenates and His-HA-tagged recombinant GRK proteins were mixed with zebrafish brain homogenate to adjust the total amounts of proteins to the same level so as to eliminate any difference between the samples in masking effects of non-GRK proteins. Note that the zebrafish brain homogenate showed no detectable immunoreactivities to the primary antibodies against GRKs. Typical immunoblot images are shown in *C*. The estimated amounts of both GRK1 and GRK7 proteins per total ocular protein are shown in *D*. Averages (also indicated as numbers) from three independent experiments are shown with SEM. Note that the GRK1 levels (left panel in *D*) contain GRK1B, which is expressed in cones (Wada *et al.* 2006). The GRK1B levels are estimated to be 0.018 ng per μg of total protein according to Wada *et al.* (2006). On the other hand, the GRK7 levels in GRK7-tg (right panel in *D*) contain GRK7 intrinsic to cones, which is estimated to be 0.15 ng per μg of total protein. After subtracting the amounts of GRK1B and GRK7 in the cones, the ratio of GRK7:GRK1 expression in the rods was estimated as 10:1 for each of the three lines of GRK7-tg animal. *E*, rhodopsin content in ocular membrane extracts estimated by spectrophotometric measurement. Averages from 10 wild-type fish, five GRK7-tg fish and four GRK1-tg fish are shown with SEM. *F* and *G*, expression levels of rod transducin α subunit (GNAT1, *F*) and rod arrestin (Arr1, *G*) in ocular homogenates. Top, typical immunoblot images from wild-type and transgenic zebrafish. Bottom, protein expression levels in the eyes of transgenic fish relative to those of wild-type. In each lane, ocular homogenate containing 3.2 μg of total protein was loaded. Averages from four to six independent experiments are shown with SEM.

Table 1. Properties of rods from WT, GRK1-tg, and GRK7-tg zebrafish

	Property	Symbol	Units	WT	GRK1-tg	GRK7-tg
Physical	OS diameter	d	μm	2.9 ± 0.1(19)	2.9 ± 0.1(13)	2.9 ± 0.1(43)
	OS length	L	μm	29.6 ± 1.2(19)	29.2 ± 0.3(13)	24.0 ± 0.6(43)*
Electrical	Dark current = maximal response	$i_D = r_{max}$	pA	5.5 ± 0.3(39)	5.0 ± 0.3(36)	5.9 ± 0.3(55)
Response *versus* intensity	Half-saturating flash intensity	$Q_{1/2}$	photons μm^{-2}	6.8 ± 0.5(39)	12 ± 1(36)*	55 ± 6(55)**
	Half-saturating photo-isomerizations	$\Phi_{1/2}$	photoiso-merizations	16	29	110
Bright flash response kinetics	Dominant time constant	$\tau_{dom,low}$	s	0.55 ± 0.03(30)	0.59 ± 0.03(26)	—
				0.57	0.41	0.54
		$\tau_{dom,med}$	s	0.95	0.92	0.96
		$\tau_{dom,high}$	s	7.5	4.1	6.1
Dim flash response kinetics	Time-to-peak	t_{peak}	s	0.57 ± 0.02(39)	0.54 ± 0.02(32)	0.84 ± 0.04(54)*
	Integration time	t_{int}	s	0.88 ± 0.04(39)	0.88 ± 0.04(33)	1.60 ± 0.07(55)*
	Decay time constant	τ_{rec}	s	0.55 ± 0.04(39)	0.53 ± 0.03(32)	1.10 ± 0.05(54)*
Single-photon response amplitude	From half-saturation intensity	a_{macro}	pA	0.23†	0.12†	0.04†
	From variance	a_{var}	pA	0.32 ± 0.02(23)	0.19 ± 0.02(11)*†	0.32 ± 0.03(14)†
	From amplitude histogram	a_{histog}	pA	0.32 ± 0.03(9)	—	0.27 ± 0.02(14)†
	Two-component analysis	a_L	pA	—	—	0.34 ± 0.02(5)
	Two-component analysis	a_S	pA	—	—	0.022 ± 0.005(5)
Effective collecting area	Physical	A_c	μm^2	2.4	2.4	2.0
	Functional	A_c	μm^2	1.95 ± 0.14(23)	1.57 ± 0.24(11)	0.32 ± 0.07(5)
Amplification constant	From single-photon response	A_{SPR}	s^{-2}	1.5 ± 0.2(23)	1.1 ± 0.2(11)	0.9 ± 0.1(17)*
	From flash family	A_{family}	s^{-2}	2.6 ± 0.3(23)	1.6 ± 0.2(11)*	1.2 ± 0.2(17)*

Physical properties and electrical response properties measured for rods of the three genotypes. Values are given as means ± SEM, except for derived values which are given without error estimates. Statistically significant differences of means from WT values are indicated: $^*P < 0.05$; $^{**}P < 0.01$. Significance was determined using Student's t test for unpaired observations; the number (n) of observations represents the number of rods tested. —: not measured. For the dominant time constant, the first row (with SEM) gives the means of the individual fits (for the lowest range of saturating intensities), whereas the values without SEM are for the slopes of the pooled data. For single-photon response amplitudes, measurements indicated † need to be treated with caution. The macroscopic values rely on the accuracy of the light intensity calibrations and on the accuracy of the calculation of effective collecting area; the values of a_{macro} for WT and GRK1-tg are about 2/3 of the estimates a_{var} and a_{histog} from variance and histogram measurements, which suggests that the actual numbers of isomerizations may have been lower than calculated from the light intensities (see Results). For GRK7-tg rods, the only estimates of single-photon response amplitude that can be considered reliable are those obtained by the two-component analysis approach.

and diameter (d) of rod outer segments (Table 1) were measured from digitized video images captured at a resolution of 5 pixels μm^{-1} with a 40× objective (LD Achroplan, Zeiss). The dimensions were indistinguishable, except for the length of GRK7-tg rods, which was almost 20% shorter than that of WT rods, giving a corresponding reduction in the 'physical' effective collecting area (A_c) of the outer segment (Table 1) that was calculated according

to eqn (14) of Baylor *et al.* (1979*b*); the 'functional' effective collecting area is considered subsequently, when we measure single-photon responses.

Expression of GRKs in transgenic rods

The cellular expression pattern of the GRK7 transgene in GRK7-tg animals is examined by immunohistochemistry in Fig. 1*B*. In the wild-type retina, GRK7 expression was restricted to cones (arrowheads), whereas in the GRK7-tg retina GRK7 was expressed both in the rod outer segments (outermost labelling) and in the cone outer segments (arrowheads).

The expression levels of GRK7 and GRK1 proteins in these transgenic lines were determined by immunoblotting of their ocular extracts (Fig. 1*C*, *D*). In GRK1-tg eyes, the level of GRK1 protein was only slightly higher than in wild-type (1.6-fold in GRK1-α and 1.8-fold in GRK1-β; Fig. 1*D* left). On the other hand, in GRK7-tg eyes, the level of GRK7 protein was substantially higher (Fig. 1*D* right), and the level of GRK1 slightly lower (Fig. 1*D* left), than in wild-type; thus, the GRK7 levels were 5.6, 5.1 and 4.1 times WT, and the GRK1 levels 0.75, 0.60 and 0.51 times WT, in the GRK7B, GRK7D and GRK7E lines, respectively. For each of the three lines of GRK7-tg animal, the ratio of GRK7 : GRK1 expression in the rods was estimated as approximately 10:1 (see legend of Fig. 1*D*). Since the molar ratio of GRK1 to rhodopsin in wild-type rods is ~1:600 (Wada *et al.* 2006), the molar ratio of GRK7 to rhodopsin in the GRK7-tg rods was estimated as ~1:60, only ~2-fold higher than the molar ratio of ~1:150 estimated in WT cones for GRKs to opsins (Wada *et al.* 2006).

The amount of rhodopsin (Fig. 1*E*) was almost unchanged in the two GRK1 transgenic lines and the GRK7E line, but was reduced in the other two GRK7 lines (to ~80% in GRK7B and to ~60% in GRK7D). These values are broadly consistent with the notion that the measured rhodopsin content was roughly proportional to the outer segment volume, which was reduced to about 80% in GRK7-tg animals, though our measurements of cell dimensions did not show clear differences between outer segment volume in the different lines of GRK7-tg animal.

We then estimated the content of several other phototransduction proteins in the eyes of transgenic zebrafish by Western blot analysis. The total amount of transducin α-subunit (Fig. 1*F*) was reduced to ~80% in the GRK1-tg eyes, and to 40–50% in the GRK7-tg eyes. After normalization to the rhodopsin content, the levels of transducin α-subunit were ~90% of WT in GRK1-tg, and 50–60% of WT in GRK7-tg. In contrast, the amounts of rod arrestin (Fig. 1*G*), rod guanylate cyclase (GC-R1), recoverin/S-modulin and RGS9 (Supplemental Fig. S1*A*, *B* and *C*, respectively) were not significantly altered among the three genotypes. Unfortunately, we do not have data on PDE, and we were not able to obtain convincing data on GCAPs.

Rhodopsin phosphorylation in retinal homogenates

GRK activity in retinas of wild-type, GRK1-tg or GRK7-tg zebrafish was analysed by our rhodopsin phosphorylation assay (Fig. 2). For retinal homogenates from each of the GRK7-tg lines the initial rate of phosphorylation of light-activated rhodopsin was significantly higher (~5.9-fold) than in wild-type, while the rate in GRK1-tg was only slightly up-regulated (~1.7-fold) compared with WT. No significant difference was observed in the phosphorylation rate among the three GRK7-tg lines.

The ~5.9-fold increase in phosphorylation rate in the GRK7-tg lines is of similar magnitude to the ~5-fold increase in GRK7 protein expression in GRK7-tg eyes (Fig. 1*C* and *D*). This is broadly as would be expected, because both sets of experiments were performed on homogenates of whole retina, which contained cones as well as rods; hence all the samples (including the wild-type controls) contained substantial endogenous GRK7. If,

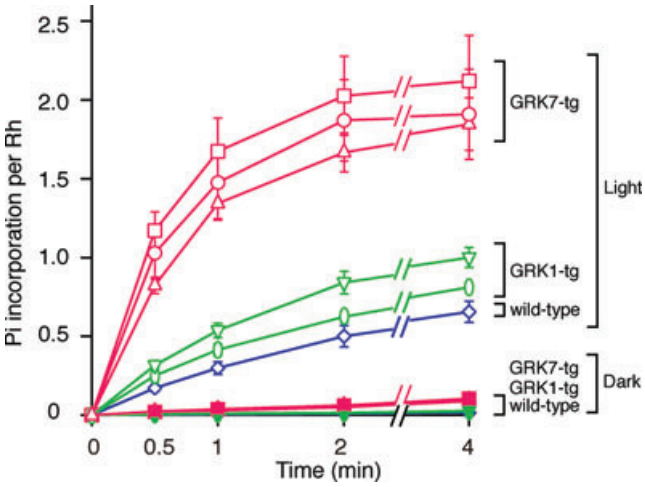

Figure 2. Time course of rhodopsin phosphorylation in retinal homogenates
Phosphorylation of rhodopsin was measured in retinas from wild-type (blue open diamonds), GRK1α (green open inverted triangles), GRK1β (green open ovals), GRK7B (red open circles), GRK7D (red open squares) and GRK7E (red open triangles) fish; open symbols denote light-exposed preparations. In darkness (filled symbols), the extent of phosphorylation was comparable to the background level and less than 10% of that for light-activated rhodopsin. For each symbol, the amount of phosphate (P_i) incorporation is averaged from three independent experiments; error bars show SEM.

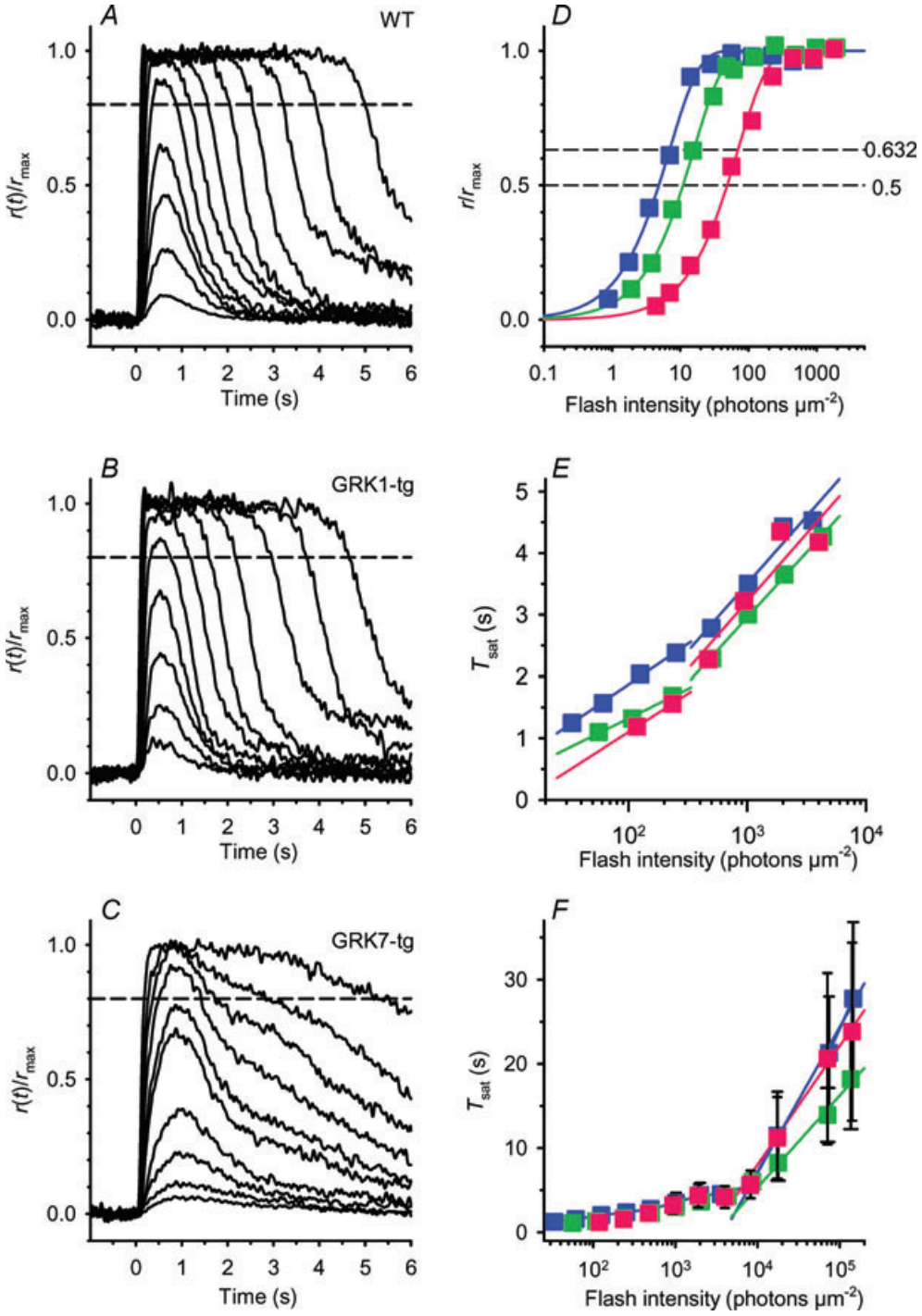

Figure 3. Families of rod photocurrents from WT, GRK1-tg and GRK7-tg zebrafish
A–*C*, response family from a representative rod for each genotype: *A*, WT; *B*, GRK1-tg; *C*, GRK7-tg. The responses shown have been normalized, and were obtained with 514 nm flashes of 1.4 ms duration delivered at time zero. Flash intensity increased by a factor of two between traces, over the range (in photons μm^{-2}): *A*, 0.9–1800; *B*, 1.8–1800; *C*, 3.5–1800. For the three cells, the circulating dark current (maximal response) was 5.5, 5.0 and 6.4 pA respectively. Dashed horizontal lines indicate the level of 20% recovery of current at which the saturation time was measured for *E* and *F*. *D*, response *versus* intensity relationships for the three rods in *A*–*C*, measured at a fixed time, just prior to the peak of the nearly saturating response: 0.45, 0.4 and 0.67 s in the three rods. Curves plot the exponential saturation function, eqn (1); the intersection of each curve with the lower and upper dashed horizontal lines give $Q_{1/2}$ and Q_e respectively. For these three rods, $Q_{1/2}$ was 4.8, 10, and 47 photons μm^{-2}. *E* and *F*, time spent in saturation, T_{sat}, plotted semi-logarithmically against flash intensity; individual points are averaged

for simplicity, one assumed the activity of GRK1 to be negligible in comparison with the activity of GRK7, then the observed ratio of phosphorylation rates in the experiments of Fig. 2 would be expected to approach the ratio of GRK7 expression levels in the different retinas in the experiments of Fig. 1, rather than the ratio of GRK7:GRK1 activities.

Circulating dark current and families of flash responses

Photoresponses generated by rods of the three genotypes were characterized using suction pipettes to record the circulating current. The qualitative form of the family of responses to flashes of increasing intensity was then analysed to determine the functional properties of the rods.

Average values of the maximal response amplitude (r_{max}, equal to the circulating dark current, i_D) for rods of the three genotypes are presented in Table 1, and were very similar to each other, at around 5–6 pA. The three lines of GRK7-tg animals showed slight differences in circulating current, but these were not statistically significant: GRK7B, 5.4 ± 0.4 ($n = 27$); GRK7D, 6.1 ± 0.3 ($n = 24$); GRK7E, 7.4 ± 0.7 ($n = 4$).

This level of circulating current is broadly as expected at this temperature (~23°C) for rod outer segments of this size, being smaller than in mammalian rods at 37°C primarily because of the powerful effect of temperature on circulating current (Baylor *et al.* 1983; Lamb, 1984; Robinson *et al.* 1993; Nymark *et al.* 2005). For comparison, at this same temperature, the mean circulating current of rat rods is only around 1 pA (Robinson *et al.* 1993).

Representative families of flash responses, normalized as $R(t) = r(t)/r_{max}$, from rods of the three genotypes are plotted in Fig. 3*A*–*C*. The waveforms recorded from WT (Fig. 3*A*) and GRK1-tg (Fig. 3*B*) rods were qualitatively similar to each other, and closely resembled the response families obtained in other species, with a uniform style of recovery from saturating responses over the illustrated range of intensities. In contrast, the waveforms obtained from GRK7-tg rods (Fig. 3*C*) were qualitatively different, exhibiting an additional kinetic component over the time-span 1–6 s for the illustrated responses. In rods of all three genotypes there was a slow component of recovery at times later than ~4 s with bright flashes (see also Supplemental Fig. S2), but the GRK7-tg rods showed different behaviour at around 3 s after the flash. It is not obvious whether this different form at ~3 s represents the addition of a slow component of recovery or the absence of a rapid component of recovery.

Response *versus* intensity relation and half-saturating flash intensity

The normalized response r/r_{max} at a fixed time was calculated from flash families as shown in Fig. 3*A*–*C*, and plotted as a function of flash intensity, Q (Fig. 3*D*). In each case the data are well described by the exponential saturation function

$$\frac{r}{r_{max}} = 1 - \exp(-Q/Q_e) \quad (1)$$

(Baylor *et al.* 1979*a*), where Q_e is the exponential saturation flash intensity, which is related to the half-saturating intensity by $Q_{1/2} = Q_e \ln 2$.

The horizontal scaling of the curves was determined by least-squares fitting, yielding values of $Q_{1/2} = 6.8$, 12 and 55 photons μm^{-2} in WT, GRK1-tg and GRK7-tg (Table 1). Compared with WT rods, the flash intensity required to half-saturate the response was nearly double in GRK1-tg rods, and about 8-fold higher in GRK7-tg rods, indicating substantially reduced sensitivities of GRK7-tg rods. In the Discussion we will comment on a range of factors that are likely to contribute to this difference in GRK7-tg rods.

Between the three lines of GRK7-tg animals, the value of $Q_{1/2}$ was roughly inversely proportional to rhodopsin content, as might be expected. Thus, for the GRK7B, GRK7D and GRK7E lines, the values of $Q_{1/2}$ (in photons μm^{-2}) were: 49 ± 6 ($n = 27$), 65 ± 12 ($n = 24$) and 35 ± 8 ($n = 4$), while in the experiments shown in Fig. 1*E* the rhodopsin levels for the corresponding lines were 2.20, 1.79 and 2.53 pmol (μg protein)$^{-1}$.

The half-saturating intensities above can be converted from units of incident light intensity to units of

from 4–32 WT, 1–29 GRK1-tg, or 3–50 GRK7-tg rods. Saturation time was measured at the 20% recovery level indicated by the dashed horizontal lines in *A*–*C* and also in Fig. S2. The fitted straight lines provide an estimate of the dominant time constant of recovery. *E*, the lower range of saturating intensities, corresponding approximately to the responses illustrated in *A*–*C*. The slope of the relationship appeared to be intensity dependent, and regression fitting has been applied separately for points below and above 500 photons μm^{-2}. For measurements below 500 photons μm^{-2}, the fitted slopes yielded values of dominant time constant, $\tau_{dom,low}$: WT, 0.57 s; GRK1-tg, 0.41 s; and GRK7-tg, 0.54 s. For measurements in the range 500–10,000 photons μm^{-2}, the fitted slopes yielded values of dominant time constant, $\tau_{dom,mid}$: WT, 0.95 s; GRK1-tg, 0.92 s; and GRK7-tg, 0.96 s. *F*, the full range of flash intensities. Regression lines fitted to the data points at flash intensities higher than 8000 photons μm^{-2} yielded the following values of dominant time constant, $\tau_{dom,high}$: WT, 7.5 s; GRK1-tg, 4.1 s; and GRK7-tg, 6.1 s. These data indicate that at extremely high intensities the rate of recovery is greatly slowed in all three genotypes.

photoisomerizations through multiplication by the respective effective collecting areas determined from the outer segment dimensions (2.4, 2.4 and 2.0 μm^2; Table 1). Hence, the numbers of photoisomerizations required to half-saturate the response were $\Phi_{1/2} = 16$, 29 and 110, for WT, GRK1-tg, and GRK7-tg, respectively.

A 'macroscopic' estimate a_{macro} for the amplitude of the single-photon response (quantal response) may be obtained by substitution into eqn (1) at an intensity of $\Phi = 1$ photoisomerization, giving

$$a_{macro} = i_D \left\{1 - \exp\left(-\ln 2/\Phi_{1/2}\right)\right\} \approx i_D \ln 2/\Phi_{1/2} \quad (2)$$

which yields values of $a_{macro} = 0.23$, 0.12, and 0.04 pA for rods of the three genotypes (Table 1). These values will be compared subsequently with estimates obtained from analysis of variance and from analysis of amplitude histograms.

Dominant time constant of recovery from saturating flashes

Analysis of the relationship between the time spent in saturation and the flash intensity has become a standard method for extracting the 'dominant time constant of recovery', τ_{dom}. Provided that the saturation time (T_{sat}) increases linearly with the logarithm of the flash intensity, then the slope of the relation gives τ_{dom} (Baylor *et al.* 1974; Pepperberg *et al.* 1992).

Representative responses are shown at relatively low saturating flash intensities (up to 1800 photons μm^{-2}) for cells of the three genotypes in Fig. 3*A*–*C*; the dashed horizontal lines denote recovery of 20% of the circulating current (at 80% of maximal response). The behaviour of the same three cells at substantially higher intensities is shown in Fig. S2.

The relationships between the saturation time and the flash intensity at the lower saturating intensities (Fig. 3*E*) or over the full range of intensities (Fig. 3*F*) were plotted in semi-logarithmic co-ordinates, for measurements averaged across each rod genotype. It is clear that the measurements cannot be explained by a single straight line over the full range of flash intensities. Instead, we chose to use straight lines over three separate regions: below 500, from 500 to 5000, and above 5000 photons μm^{-2}. For the lowest of these intensity regions the slopes of the regression lines correspond to a $\tau_{dom,low}$ of 0.57 and 0.41 s for WT and GRK1-tg rods (see Fig. 3*E*). For GRK7-tg rods the responses only just reached saturation at these intensities, so it is difficult to estimate the slope accurately; however it appears to be roughly similar, at 0.54 s (Fig. 3*E*). For the mid-region of intensities, the slope was very similar between the three genotypes and about double that at the lower intensities, with the dominant time constant in this region ($\tau_{dom,mid}$) being 0.95 s, 0.92 s and 0.96 s for WT, GRK1-tg and GRK7-tg rods respectively (Fig. 3*E*). For the three lines of GRK7-tg animals, the values of $\tau_{dom,mid}$ were similar between GRK7B (1.02 ± 0.11 s, $n = 20$) and GRK7D (0.96 ± 0.05 s, $n = 24$), but significantly shorter in GRK7E (0.70 ± 0.03, $n = 4$; $P < 0.05$, *t* test for samples of unequal variance).

At the highest region of saturating flash intensities there were substantial inter-cell differences (note large error bars in Fig. 3*F*), but on average the slope was considerably steeper, corresponding to longer dominant time constants of 7.5 s, 4.7 s and 6.1 s for WT, GRK1-tg and GRK7-tg rods, respectively. The apparent changes in the slope of the relationship between T_{sat} and the flash intensity suggest that the rate-limiting step that governs the overall rate of recovery of the circulating current is dependent on the number of photoisomerizations elicited by the flash.

In view of the scatter in the data, we think that the slopes determined in the lowest and highest intensity regions may not be very reliable. On the other hand, the slopes in the middle region of intensities (e.g. for saturation times of roughly 2–5 s) are likely to be more reliable, and our measurements indicate that in this region there is little difference in the dominant time constant between the three genotypes, with each being close to 1 s. This might indicate that in this middle region the dominant time constant is determined by the lifetime of activated transducin/PDE rather than by the rhodopsin lifetime.

For GRK1-tg zebrafish, the lack of an obvious change in dominant time constant in the middle region of intensities is consistent with the results of Krispel *et al.* (2006) in mouse rods, where over-expression of GRK1 had little effect on τ_{dom}. On the other hand, our results suggest that in both the lower and higher intensity regions the time constant may be somewhat shorter in GRK1-tg rods than in either WT or GRK7-tg rods, as might be expected if the dominant time constant in those regions was set by the level of GRK1; however, these are the regions where the data are least reliable.

As a further indicator of response time-course, we attempted to measure the kinetics of the $Na^+/Ca^{2+},K^+$-exchange current in the bright-flash responses, but we were unable to resolve this component of current in our recordings. Representative responses to intense flashes are illustrated in Supplemental Fig. S2 on a slow time base, and inspection of the traces shows no obvious sign of any resolvable component of exchange current. Thus we cannot provide information on the kinetics of changes in intracellular Ca^{2+} concentration in zebrafish rods.

Kinetics of dim flash responses

Responses to dim flashes were recorded from representative rods of each genotype (Fig. 4*A*–*C*) and

averaged responses across each genotype are shown in Fig. 4*D*. In each case, the 'dim' flash was one eliciting a response of ∼10% of maximum; because of the lower sensitivity of the GRK7-tg rods, the flash intensity required was 5–10 times higher than for WT rods. The curves fitted in Fig. 4 are the 'Poisson kinetics' function used previously for toad rods by Baylor *et al.* (1979*a*) as their eqn (3)

$$r(t) \propto t^{n-1} \exp(-t/\tau) \tag{3a}$$

$$\frac{r(t)}{r_{\text{peak}}} = \left(\frac{t}{t_{\text{peak}}}\right)^{n-1} \exp\left[(n-1)\left(1-\frac{t}{t_{\text{peak}}}\right)\right]. \tag{3b}$$

Here n is the Poisson exponent representing the number of cascaded stages of equal time constant. The first unscaled form, eqn (3a), uses that time constant, τ, to characterize the response time course. In the second form, eqn (3b), the response $r(t)$ is normalized to a peak amplitude of r_{peak} which occurs at a time-to-peak of t_{peak} that is given by $t_{\text{peak}} = (n-1)\tau$.

For WT (Fig. 4*A*) and GRK1-tg (Fig. 4*B*) rods, we obtained good fits with $n = 4$ and with values for t_{peak} of around 0.6 s. For GRK7-tg rods (Fig. 4*C*), the responses were more asymmetric, requiring a smaller (and sometimes non-integer) exponent n of 2–3, together with a longer time-to-peak. For the populations of rods from which we recorded, the dim flash times-to-peak were 0.57, 0.54 and 0.84 s for WT, GRK1-tg and GRK7-tg genotypes (Table 1). We also measured the integration time (t_{int}) defined as the area under the flash response divided by its amplitude, as well as the time constant of the recovery phase (τ_{rec}) which we determined by fitting an exponential to the tail of the response below half-maximal. These parameters were closely similar between WT and GRK1-tg rods, but were both roughly double in GRK7-tg rods (Table 1).

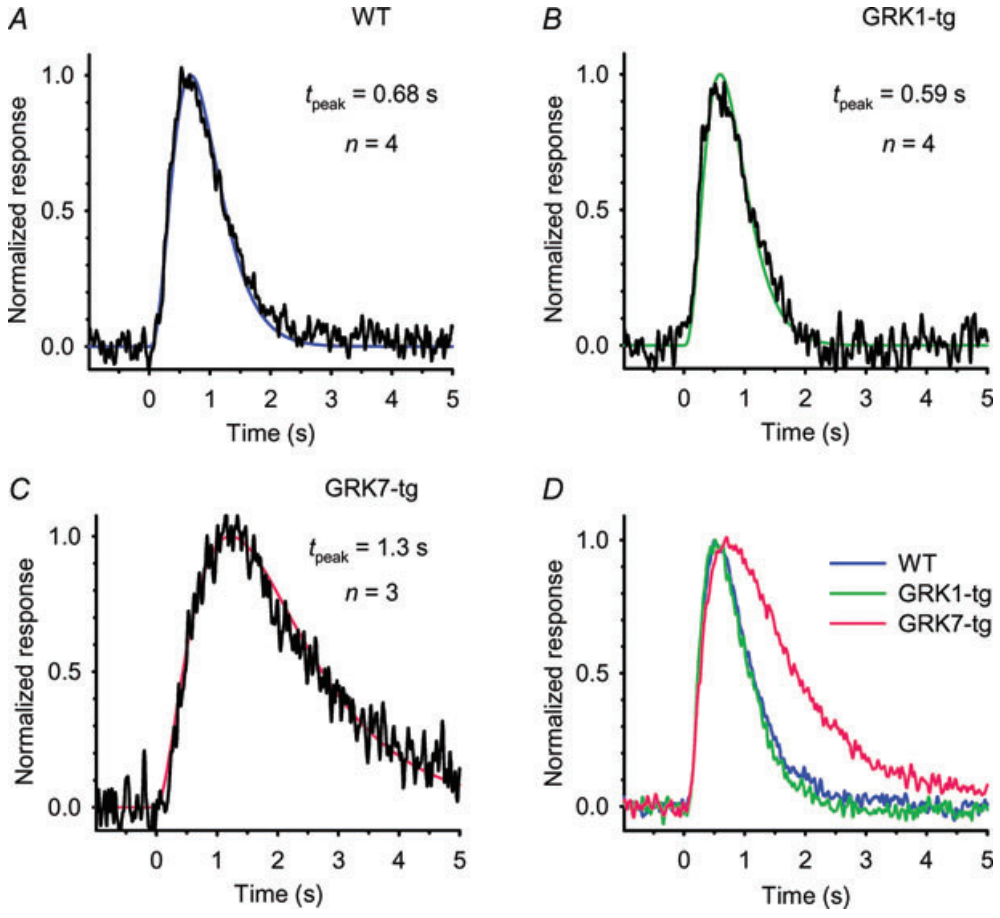

Figure 4. Dim-flash response kinetics for rods of the three genotypes
A–C, dim-flash responses from a representative rod of each genotype: *A*, WT; *B*, GRK1-tg; *C*, GRK7-tg. The responses have been normalized to unit amplitude, and have been fitted with the kinetic form of eqn (3) with the parameters t_{peak}, n, and r_{peak} set as follows: *A*, WT: 0.68 s, 4, 0.51 pA; *B*, GRK1-tg: 0.59 s, 4, 1.3 pA; *C*, GRK7-tg: 1.3 s, 3, 0.59 pA. *D*, population mean responses for rods of the three genotypes. Normalized responses from the individual rods were averaged across each genotype, and then re-normalized (to compensate for the reduction that occurred because of dispersion in t_{peak}). The mean and SEM for the time-to-peak (and the number of rods averaged) are listed in Table 1.

These results show the unexpected finding that the lowered photosensitivity of rods expressing the cone-specific GRK7 was accompanied by *slower* kinetics of the dim flash responses, whether measured by the time-to-peak (t_{peak}), the integration time (t_{int}), or the decay time constant (τ_{rec}). In the Discussion, we consider possible mechanisms that might contribute to this slowing of the dim-flash responses. For responses to saturating flashes, though, the dominant time constant of recovery ($\tau_{dom,low}$ and $\tau_{dom,med}$) in GRK7-tg rods was not obviously longer than in the other two genotypes. As mentioned above, the qualitative shape of the family of flash responses in GRK7-tg rods (Fig. 3*C*) differed from those obtained in WT and GRK1-tg rods.

The single-photon response: three approaches

We used three approaches for estimating the single-photon response of the rods. (i) First, the macroscopic approach, in which we substituted the dark current i_D and half-saturating intensity $\Phi_{1/2}$ into eqn (2), to give the values listed in Table 1; however, this approach relies heavily on the accuracy of our estimates of the effective collecting area and our calibrations of the light intensity. Two other approaches are standard in the literature: (ii) analysis of the variance of the responses to dim flashes, and (iii) measurement of the histogram of the amplitude distribution for very dim flashes (Baylor *et al.* 1979*b*; Rieke & Baylor, 1998; Whitlock & Lamb, 1999; Burns *et al.* 2002; Hamer *et al.* 2003). These conventional approaches are illustrated for WT and GRK7-tg rods in Figs 5 and 6 and for GRK1-tg rods in Supplemental Fig. S3.

We would point out that this analysis is made difficult by the small size of the single-photon response (<0.3 pA) that accompanies the small amplitude of the circulating dark current (~6 pA) in zebrafish rods at room temperature. As a result, the signal-to-noise ratio of the recordings is poorer than in experiments on cells with larger photocurrents. While we achieved reasonable success with the variance analysis approach, we experienced difficulty obtaining reliable histograms for single-photon responses of such small amplitude.

Single photon responses of WT zebrafish rods

Our recordings from rods of WT zebrafish demonstrated single photon responses broadly comparable to those found in other species. An experiment on a representative rod stimulated with a long series of very dim flashes is

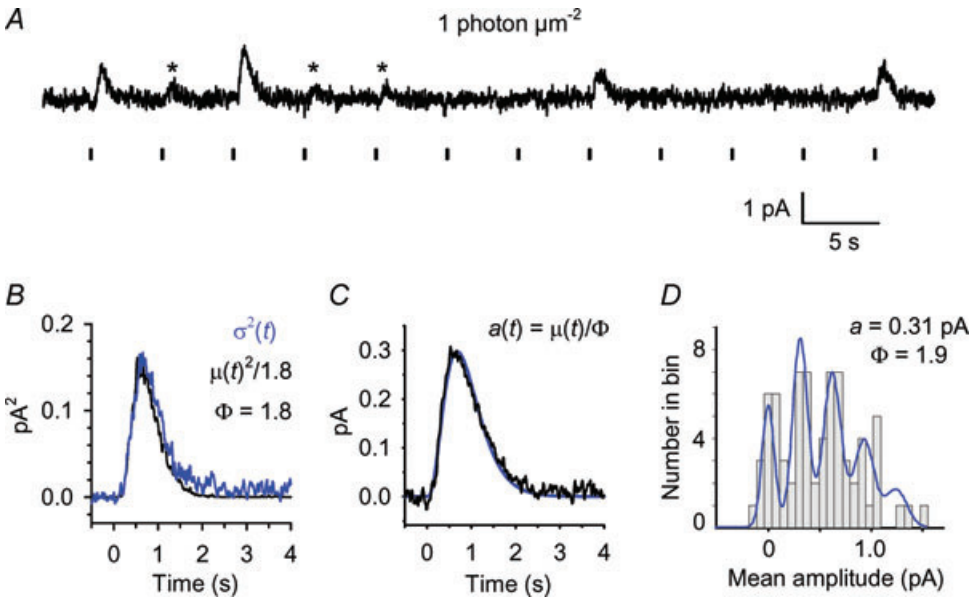

Figure 5. Analysis of quantal responses in a WT rod
A, set of 12 consecutive responses from a WT rod for flashes of fixed dim intensity (~1 photon μm^{-2}) delivered at 5 s intervals, as indicated by vertical markers below the trace. Presumed unitary events (single photon responses) are indicated by asterisks. *B–D*, variance analysis and histogram analysis on 73 responses of the kind illustrated in *A*. *B*, ensemble variance, $\sigma^2(t)$ (blue trace), together with a scaled version of the square of the mean response, $\mu(t)^2$ (black trace); with a scaling factor of 1/1.8 the two traces coincided closely, yielding an estimate for the number of photoisomerizations as $\Phi = 1.8$; see eqn (4a). *C*, estimated quantal response, $a(t)$, obtained by dividing the mean response by the estimate for Φ; see eqn (4b). The blue curve plots the Poisson kinetics of eqn (3), with amplitude $r_{peak} = 0.3$ pA, $t_{peak} = 0.68$ s, and $n = 4$. *D*, amplitude histogram for the 73 responses, measured over a window 0.5 s wide centred at t_{peak}, and using a bin width of 0.05 pA. The blue curve plots the sum of Poisson-weighted Gaussian components, as described in eqn (10) of Baylor *et al.* (1979*b*), using parameters: $a = 0.31$ pA; Φ ($= m$) $= 1.9$; $\sigma_0 = 0.045$ pA; $\sigma_1 = 0.045$ pA.

illustrated in Fig. 5, and average parameters from WT rods are presented in Table 1.

The sample of 12 dim flash responses in Fig. 5*A* exhibits classical photon fluctuations, with apparent failures interspersed between apparent singletons (marked by asterisks) and larger events presumed to be multiple photon hits. For a long series of such responses, the ensemble variance $\sigma^2(t)$ was found to be proportional to the square of the ensemble mean response $\mu(t)$ (Fig. 5*B*), as expected if the variance is dominated by the quantal nature of photon absorption. The mean number of photoisomerizations per flash, Φ, and the mean quantal event, $a(t)$, were estimated from the required scaling in the usual way, using the equations

$$\sigma^2(t) = \mu(t)^2/\Phi \tag{4a}$$

and

$$a(t) = \mu(t)/\Phi. \tag{4b}$$

For the traces in Fig. 5*B*, the required scaling of mean squared to variance gave $\Phi = 1.8$; the single photon response plotted in Fig. 5*C* had an amplitude of 0.3 pA and was well fit by the Poisson kinetics expression of eqn (3). For 23 WT rods we obtained the mean amplitude of the single photon response, estimated from variance analysis, as $a_{\text{var}} = 0.32 \pm 0.02$ pA (Table 1).

We also applied conventional amplitude histogram analysis to the same set of dim flash responses, as illustrated in Fig. 5*D*. We found that the shape of the histogram was sensitive to the bin width chosen (because of the finite number of responses per bin), so that the form of the histogram was not especially robust. Nevertheless, for nine WT rods, using bin widths of 0.055–0.075 pA, the distribution featured equidistant peaks and could be fit satisfactorily with the theoretical curve expected for a Poisson-distributed sum of Gaussians; i.e. by eqn (10) of Baylor *et al.* (1979*b*). In performing such fitting, we began with the values for a and Φ (termed m in the original formulation) determined from the variance analysis (as above), and we manually adjusted the widths of the Gaussians, described by the parameters σ_0 and σ_1, representing the standard deviations of the failures peak and the unitary peak, respectively. We subsequently allowed minor adjustment of the parameters a and Φ. For the WT cell illustrated in Fig. 5, a good fit to the histogram was obtained using $a = 0.31$ pA and $\Phi = 1.9$, together with the other parameters listed in the legend. For the nine WT rods, the mean value of quantal amplitude that we obtained for the single photon response, from the histogram fitting was $a_{\text{histog}} = 0.32 \pm 0.03$ pA (Table 1).

Single photon responses of GRK1-tg zebrafish rods

Comparable dim flash analysis for a GRK1-tg rod is illustrated in Fig. S3. Because the sensitivity of GRK1-tg rods was roughly 0.5 that of WT rods (Fig. 3*D*) we anticipated that the amplitude of the single photon response would be about half that determined above for WT rods. In Fig. S3*B*, the scaling required to bring the mean-squared response into alignment with the variance corresponded to $\Phi = 2.4$, and the scaled response in Fig. S3*C* provided an estimate for the amplitude of the single photon response of 0.16 pA. For 11 GRK1-tg rods, the mean value for the amplitude of the single photon response, estimated from variance analysis, was $a_{\text{var}} = 0.19 \pm 0.02$ pA (Table 1), which is significantly ($P < 0.05$) smaller than the value of 0.32 pA for WT rods.

For the cell depicted in Fig. S3, the amplitude histogram (Fig. S3*D*) showed a suggestion of multiple peaks, and could be fit by the sum of Gaussians formulation using parameter values of $a = 0.17$ pA and $\Phi = 2.25$, quite similar to the values estimated above from the variance analysis. Although the fit of the curve in Fig. S3*D* is respectable, we do not regard it as providing particularly strong evidence for the magnitude of the quantal event. Because of the smaller amplitude of the underlying quantal event in GRK1-tg rods, in the presence of a similar level of recording noise, we were unable to rely on the histogram approach for rods of this genotype.

In comparing the estimated amplitudes of the single-photon events between WT and GRK1-tg rods obtained using the different approaches, we note that the macroscopic value (a_{macro}) is ~2/3 that of the estimates

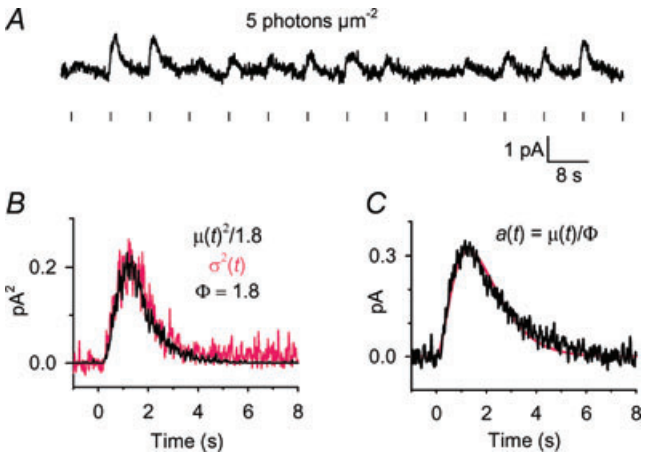

Figure 6. Conventional analysis of quantal responses in a GRK7-tg rod
A, sample of 14 consecutive responses from a set of 30 responses obtained at an intensity of ~5 photons μm^{-2}. *B*, ensemble variance, $\sigma^2(t)$ (grey trace), together with a scaled version of the square of the mean response, $\mu(t)^2$ (black trace); with a scaling factor of 1/1.8 the two traces coincided closely, yielding an estimate for the number of photoisomerizations as $\Phi = 1.8$; see eqn (4a). *C*, estimated quantal response, $a(t)$, obtained by dividing the mean response by the estimate for Φ; see eqn (4b). The smooth curve plots the Poisson kinetics of eqn (3), with amplitude $r_{\text{peak}} = 0.31$ pA, $t_{\text{peak}} = 1.3$ s, and $n = 3$.

from the variance and histogram methods (a_{var} and a_{histo}). We presume that the smaller size of the macroscopic estimate stems from a slight but systematic error in the calculation of photoisomerizations, resulting either from a calibration error in the incident light intensities, or from a shortcoming in the estimate of effective collecting area. We conclude that for WT and GRK1-tg zebrafish rods the mean amplitude of the response to a single photoisomerization of a rhodopsin molecule is about 0.3 pA and 0.2 pA, corresponding to suppression of about 6% and 4% of the circulating dark current.

Single photon responses of GRK7-tg zebrafish rods: conventional analysis

Single-photon response analysis is possible when the amplitude of the quantal event is reasonably large in comparison with the instrumental recording noise. For rods of GRK7-tg zebrafish, which exhibited low sensitivity, and for which the apparent (macroscopic) quantal event, a_{macro}, was roughly six times smaller than for WT rods, we anticipated that detection of quantal events might be difficult. Experiments using a similar flash intensity to that in Fig. 5 confirmed that little could be resolved with low intensity flashes (see Supplemental Fig. S4). At this low intensity, the mean response was small (around 0.05 pA) and almost no response variability could be detected; thus, the variance trace showed no obvious time-dependence (Fig. S4*C*). However, we found that by using a higher flash intensity (for example, 5-fold higher in the experiment in Fig. 6 than for WT rods), we were able to detect quantal fluctuations.

Although there was substantial variability in the response amplitudes obtained for a series of identical dim flashes, it was not clear from inspection whether any response failures were present within the set of responses (Fig. 6*A*). The variance trace $\sigma^2(t)$ in Fig. 6*B* exhibited a substantial time-dependent component, whose time course was synchronous with that of the mean-squared response $\mu(t)^2$, with a vertical scaling corresponding to $\Phi = 1.8$. Using this value of Φ, the presumed single-photon response, $a_{var}(t)$ (Fig. 6*C*), had an amplitude of 0.31 pA. However, as the analysis in the next section illustrates, these estimates are not reliable.

Two classes of quantal response for rods of GRK7-tg zebrafish?

The finding of substantial variability (Fig. 6*B*), yet the absence of obvious responses with zero amplitude (Fig. 6*A*), led us to suspect that the responses might comprise the combination of a relatively constant underlying response waveform together with a superimposed fluctuating response. In particular, we wondered whether two classes of response might be present simultaneously: namely, a few larger 'quantal' events (giving variability), superimposed on a roughly constant response resulting from a substantial number of quite small events. To investigate this idea, we needed to formulate an explicit proposal that the responses of GRK7-tg rods comprise the sum of two kinds of event, and then we needed to test whether the recorded responses display the properties expected from such a model.

Two-component model. We examined the hypothesis that the dim flash responses of rods from GRK7-tg zebrafish represents the sum of two components:

$$r(t) = r_L(t) + r_S(t) \quad (5)$$

where $r_L(t)$ and $r_S(t)$ are the responses to the larger and smaller events, possibly contributed by activated rhodopsin molecules (Rh*) that are shut-off by GRK1 and GRK7, respectively (see Discussion). For simplicity, we made two assumptions. Firstly, we assumed that the variance arising from the smaller events is negligible compared with that from the larger events, i.e. that $\sigma_S^2(t) \approx 0$. This means that each of the small responses has exactly the same amplitude and time course; i.e. that $r_S(t) = \mu_S(t) = \Phi_S a_S(t)$ where Φ_S is the number of isomerizations eliciting 'small events' and $a_S(t)$ is their elementary amplitude. Secondly, we assumed (as previously) that the variance of the larger responses is dominated by the Poisson nature of photoisomerizations, i.e. that fluctuations about the mean quantal amplitude may be ignored.

Predictions of two-component model. On this basis, we would expect to be able to describe the amplitude histogram for dim flash responses from a GRK7-tg rod as the theoretical curve for the large (quantal) responses plus an offset corresponding to the fixed size (at this intensity) of the small responses. A trace calculated in this way provided a good fit to the observed histogram (Fig. 7*B*). As explained below, this curve has an offset of $\mu_S = 0.18$ pA (corresponding to the invariant amplitude of the small responses), while the large events had a quantal amplitude of $a_L \approx 0.22$ pA.

Protocol. A sample of 10 out of the 76 raw responses obtained at a fixed low flash intensity is shown in Fig. 7*A*, and the ensemble mean of all 76 responses is plotted as $\mu_T(t)$ in Fig. 7*C*. We first needed to obtain an estimate of the response elicited by the small events alone. Then, by subtraction, we could obtain the set of larger responses.

The amplitude of each of the 76 individual raw responses was determined by least-squares fitting of eqn (3), with $n = 2.5$ and with t_{peak} allowed to vary. The resulting amplitude histogram (Fig. 7*B*) exhibited a first

peak near 0.2 pA together with a dip near 0.3 pA and another peak near 0.4 pA.

Mean response elicited by the smaller events. In order to obtain an estimate of the smaller responses alone (i.e. those responses making up the left-most peak in the histogram), we chose to set a selection window symmetrically around that peak (from 0.08–0.28 pA, see linked arrows in Fig. 7*B*); within this window there were 32 responses. The mean of those 32 responses (Fig. 7*C*) was taken as an estimate of the (constant) smaller response at this flash intensity, i.e. an estimate of $r_S(t) = \mu_S(t)$. The time

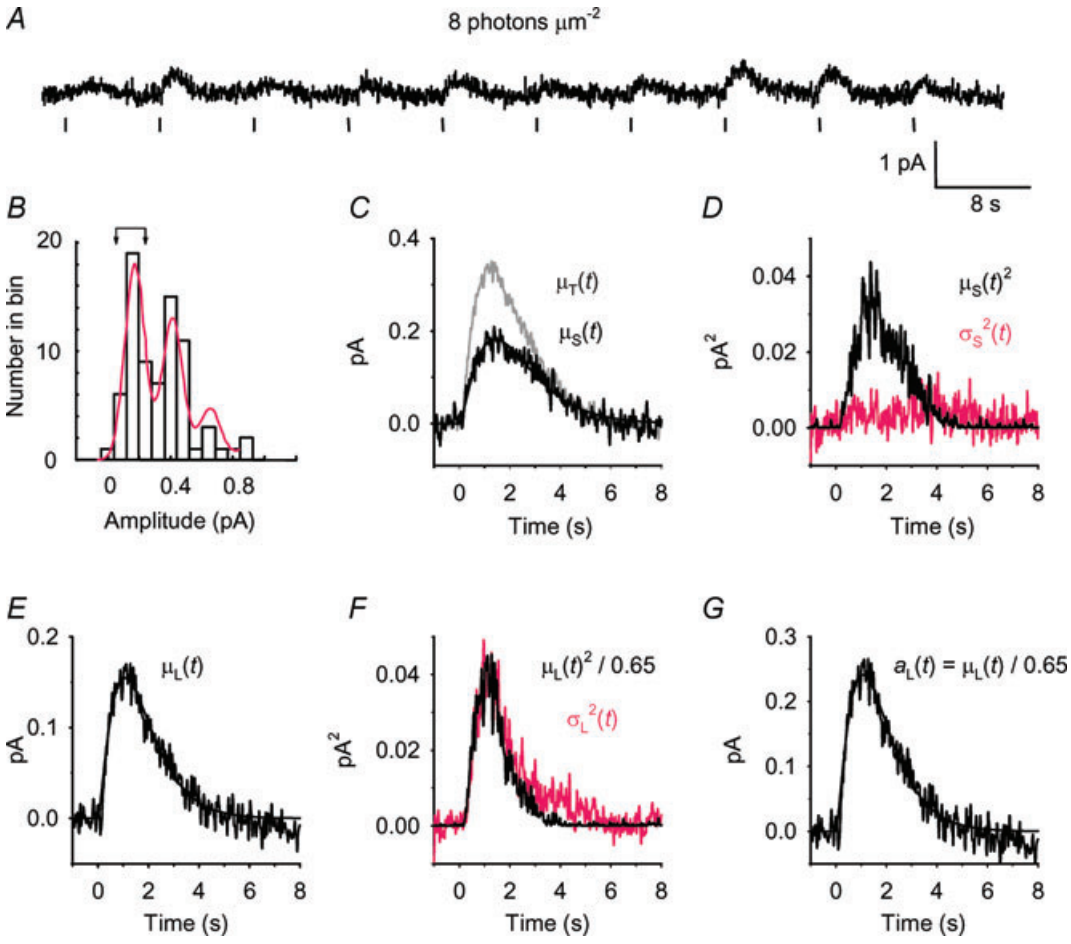

Figure 7. Two component analysis of GRK7-tg rod responses
A different rod from a GRK7-tg zebrafish was stimulated with a series of 76 flashes delivering ~8 photons μm^{-2}. *A*, sample consecutive responses. The amplitude of each individual response was determined by least-squares fitting each trace with eqn (3) (with $n = 2.5$ and with t_{peak} constrained to be in the range 1.0–1.5 s). *B*, amplitude histogram for the 76 responses, plotted using a bin width of 0.077 pA. The smooth curve plots a laterally shifted sum of Poisson-weighted Gaussian components, with an offset of 0.182 pA (see Results), and with remaining parameters: $a = 0.23$ pA; $\Phi = 0.99$; $\sigma_0 = 0.062$ pA; $\sigma_1 = 0.045$ pA. *C* and *D*, analysis of 'small responses', defined as those responses with an amplitude lying between the lower and upper threshold levels of 0.08 and 0.28 pA indicated in the amplitude histogram in *B*. *C*, ensemble mean $\mu_T(t)$ of all 76 responses, together with ensemble mean $\mu_S(t)$ of the selected small responses (32 from 76 responses); the curve fitted to $\mu_S(t)$ is the Poisson kinetics of eqn (3), with $r_{peak} = 0.18$ pA, $t_{peak} = 1.4$ s, and $n = 2.5$. *D*, ensemble variance $\sigma_S^2(t)$ for the same selected responses (red trace), compared with the square of the ensemble mean $\mu_S(t)^2$ (black trace) from *C*. *E* and *F*, analysis of responses to the 'large events', defined as the 76 raw traces after subtraction of the mean small response $\mu_S(t)$ determined in *C*. *E*, ensemble mean of the large responses, $\mu_L(t)$. *F*, ensemble variance of the large responses, $\sigma_L^2(t)$ (red trace), together with a scaled version of the square of the mean of the large responses, $\mu_L(t)^2$ (black trace); with a scaling factor of 1/0.65 the two traces coincided, yielding an estimate for the number of photoisomerizations underlying the large responses of $\Phi = 0.65$; see eqn (4a). *G*, estimated quantal response of the 'large events', $a_L(t)$, obtained by dividing the mean response in *E* by the estimate for Φ; see eqn (4b). $a_L(t)$ was fit with the Poisson kinetics of eqn (3), with $r_{peak} = 0.24$ pA, $t_{peak} = 1.04$ s, and $n = 2.5$. For this cell, the macroscopic sensitivity was lower than in other GRK7-tg rods, with $Q_{1/2} \approx 100$ photons μm^{-2} compared with the mean of 55 photons μm^{-2} (Table 1).

course of this response was well described by eqn (3) with $r_{peak} = 0.18$ pA, $t_{peak} = 1.4$ s, and $n = 2.5$. The variance trace $\sigma_S^2(t)$ in red had no obvious component synchronous with the mean-squared trace, $\mu_S(t)^2$ (Fig. 7*D*), as expected if these selected small-amplitude traces are indeed drawn from a distribution with negligible variance. It needs to be emphasized that these small responses with an amplitude of ~0.18 pA were not single-photon responses; instead we presume them to be responses to a substantial number Φ_S of isomerizations that generated very small quantal events, $a_S(t)$. As the test flash intensity was 8 photons μm^{-2} and the effective collecting area was 2.0 μm^2 (Table 1), we estimate $\Phi_S \approx 16$ isomerizations, so that the amplitude of the underlying small events would have been $a_S \approx 0.012$ pA in this cell.

Mean response elicited by the larger events. We next determined the raw responses that remained in the absence of the small responses; i.e. we estimated the individual 'large responses' (including both failures and successes). Thus, from the assumption in eqn (5) that each of the raw responses includes a (variable) large response plus the fixed mean of the smaller responses, we took each of the raw traces and subtracted the Poisson curve (eqn (3)) that had been fit to $\mu_S(t)$, to obtain the set of larger responses, $r_L(t)$. The mean, $\mu_L(t)$, of these larger responses is plotted as the noisy trace in Fig. 7*E*. This trace is an estimate of the mean response to some (as yet unknown) number Φ_L of the larger (quantal) events $a_L(t)$; i.e. it is an estimate of $\mu_L(t) = \Phi_L a_L(t)$.

Size and number of the larger events. Next, we applied variance analysis to the entire ensemble of responses (Fig. 7*F*). Given that we assumed the variance of the responses to the small events to be negligible, $\sigma_S^2(t) \approx 0$, then the variance $\sigma^2(t)$ for the entire ensemble (red trace) will represent the variance $\sigma_L^2(t)$ contributed by the large responses alone. Accordingly, we compared this variance trace with a scaled version of the square of the mean response to the large events, $\mu_L(t)^2$ (black trace). The required vertical scaling in Fig. 7*F* corresponds to a mean number of larger events of $\Phi_L = 0.65$. Finally we divided the mean $\mu_L(t)$ by this value of Φ_L to obtain our estimate for the larger (quantal) events, $a_L(t)$ (Fig. 7*G*). This trace had an amplitude of $a_L = 0.24$ pA, and was fit with eqn (3) using $t_{peak} = 1.04$ s and $n = 2.5$. For comparison, application of conventional variance analysis (assuming only a single class of event) to the same flash responses yielded quite different values, $a = 0.16$ pA and $\Phi = 2.2$.

Conformity to predictions. Having applied this analysis, we needed to check whether the experimental observations conform to the predictions of the two-component model, and we found no grounds for rejecting the hypothesis. First, the variance of the presumptive small responses was close to zero (Fig. 7*D*), as predicted. In addition, the first peak ('large failures') in the amplitude histogram (Fig. 7*B*) had an offset of 0.182 pA, consistent with the value of 0.18 pA predicted from the mean amplitude of the presumptive small events. Finally, the spacing between the peaks in the amplitude histogram of ~0.23 pA (Fig. 7*B*) is broadly consistent with the amplitude a_L of the large events of 0.24 pA (Fig. 7*G*), and moreover the histogram is reasonably well described by the theoretical curve.

Collected measurements for GRK7-tg rods. Overall, for GRK7-tg zebrafish, we were able to apply conventional variance analysis and histogram analysis to 14 rods. However, the interpretation of this analysis is limited by three factors: (i) the poor signal-to-noise ratio associated with the small quantal event amplitude, (ii) the likely shortcomings of the conventional analysis, if it is indeed the case that more than one class of quantal event exists in GRK7-tg rods, and (iii) the finite numbers of responses that we were able to obtain (from 30–196) in different cells. Using the conventional variance approach (Fig. 6), the mean amplitude of the events in a single-component description was obtained as $a_{var} = 0.32 \pm 0.032$ pA (14 rods). Using histogram analysis of GRK7-tg rods (Fig. 7*B*), it appeared that the 'failures' peak was always offset positively from 0 pA, and for the 14 rods this offset averaged approximately 0.2 pA. In contrast, for 23 WT rods, no such offset was required in fitting the amplitude histogram, and the 'failures' peak always appeared to be centred at 0 pA (see, for example, Fig. 5*D*). In addition, for each of the GRK7-tg cells, the separation between the peaks in the histogram appeared quite similar to the estimate of quantal amplitude obtained using the variance method in the same cell, and from the curves that we fitted to the amplitude histograms we obtained a mean quantal amplitude of $a_{histog} = 0.27 \pm 0.03$ pA (14 rods).

Thus, in all 14 GRK7-tg rods that we analysed, the values of a_{var} and a_{histog} were comparable to those obtained in WT rods, yet the 'failures' peak was always offset from zero. For five of these 14 rods we were successfully able to apply the separation of components analysis, and we obtained the mean amplitude of the larger (quantal) events as $a_L = 0.34 \pm 0.02$ pA. For the remaining nine cells we have no reason to doubt the existence of two components, but because of the relatively poor signal-to-noise ratio associated with sub-picoamp responses, combined with the more demanding processing required for the separation of components approach, we were not able to apply that analysis successfully.

This estimate of $a_L = 0.34 \pm 0.02$ pA for the 'larger' quantal event amplitude in the five GRK7-tg rods is only marginally greater than the conventional estimates, of a_{var} and a_{histog}, in the 14 GRK7-tg rods, but for the reasons

set out above we regard it as being likely to be a more reliable estimate. For the same cells, the mean offset (response to the smaller events) was 0.28 ± 0.05 pA, and from the flash intensities used the mean amplitude of the smaller events was estimated $a_S = 0.022 \pm 0.005$ pA (see Table 1). The mean value of the ratio of event amplitudes was $a_L/a_S = 16 \pm 2.3$. Other mean parameters from our experiments on these five rods were: $\Phi_L = 0.6 \pm 0.1$, $\Phi_S = 13.3 \pm 1.7$, and the ratio $\Phi_S/\Phi_L = 22 \pm 1.5$.

Amplification constant of phototransduction

The amplification constant, A, characterizing the cascade of phototransduction reactions can be determined from the electrical response, provided that a reliable estimate is available for the number of photoisomerizations elicited by the flash of light (Lamb & Pugh, 1992; Pugh & Lamb, 1993). The intensity calibration is unambiguous when the single-photon response is known.

Amplification constant from single-photon responses. For dim flashes, the generalized equation for the rising phase of the response simplifies to

$$R(t) = \frac{1}{2}\Phi A(t - t_{\text{eff}})^2 \qquad (6)$$

where $R(t) = r(t)/r_{\max}$ is the fractional response, Φ is the number of photoisomerizations, and t_{eff} is an effective delay time that combines a number of short delays in phototransduction together with a delay caused by electrical filtering (Lamb & Pugh, 1992; Pugh & Lamb, 1993). In the special case of the single-photon response, we have $\Phi = 1$. The magnitude of the delay time t_{eff} can best be determined from the fit obtained for responses to flashes of higher intensity (see below).

Figure 8*A* plots single-photon responses, determined by using variance analysis and then normalized as a fraction of the circulating current, for three representative cells. These fractional responses, $R(t)$, were fit with the parabolic rise predicted by eqn (6); to minimize the distorting effects of inactivation steps, the fitting was restricted to times earlier than 250 ms after the flash. The fitted values of the amplification constant (obtained with $\Phi = 1$) for these three cells were $A = 1.5$, 0.8 and 1.2 s^{-2} for WT, GRK1-tg and GRK7-tg, respectively. The mean values of A for cells of the three genotypes are collected in Table 1, and were 1.5, 1.1 and 0.9 s^{-2}. From the flash intensity used to elicit the single-photon responses, we calculated 'functional' effective collecting area; thus, if the number of photoisomerizations was determined as Φ for a flash delivering Q photons μm^{-2}, then the functional collecting areas was calculated as $A_c = \Phi/Q$. We obtained $A_c = 1.99$, 1.8 and 0.08 μm^2 for the illustrated cells and means of $A_c = 1.95$, 1.57 and 0.32 μm^2 for cells of the three genotypes (see Table 1); note that the small value of functional collecting area in GRK7-tg rods applies for eliciting the 'large events'.

Amplification constant from flash family responses. Figure 8*B–D* plots families of responses, from dim to saturating flashes, for the same three cells whose single-photon responses were analysed in Fig. 8*A*. A relatively fast time scale was used, to emphasize the onset phase of the responses. Each family of responses was fit as an ensemble, using the prediction of the Lamb & Pugh model filtered by the cell's capacitive time constant (as described by equation (5) of Smith & Lamb (1997); the numbers of photoisomerizations Φ were calculated from the light intensity calibrations together with the effective collecting areas determined above from the single-photon responses. From the fits for the responses to brighter flashes, we constrained the capacitive time constant to $C_m = 5$ ms and the residual delay to 43 ms (giving a total effective delay time in Fig. 8*A* of $t_{\text{eff}} = 48$ ms). The quality of the ensemble fit to the rising phase of the responses was good for the rods of each genotype. The amplification constants derived from the ensemble fitting to the flash families were 1.8, 1.0 and 1.4 s^{-2} for the WT, GRK1-tg and GRK7-tg rods, respectively, slightly higher than the values obtained above for the fits to the single-photon responses. The difference between the sets of estimates probably arose from the fact that the single-photon responses were fit to a somewhat later time (250 ms) than is strictly justified by the requirement in the Lamb & Pugh model that inactivation reactions must not have set in.

The mean values of the amplification constant for rods of the three genotypes are listed in Table 1. For GRK1-tg rods, the amplification constant was about two-thirds that in WT rods, while in GRK7-tg rods it was about half that in WT rods. These values accord reasonably with the observed changes in transducin (GNAT1) expression levels shown in Fig. 1*F*, of roughly 1:0.9:0.5, as expected if the differences in amplification constant simply reflect differences in transducin levels in the outer segments (see Discussion).

Optokinetic response in transgenic zebrafish

To test whether the expression of GRK7 in rods affects the visual performance of zebrafish, larvae from one of the GRK7-transgenic lines (GRK7B) were subjected to a behavioural test based on the optokinetic response (OKR). Most previous studies of OKR in larval zebrafish have employed bright light conditions aimed at analysing photopic (cone) vision (Brockerhoff *et al.* 1995; Neuhauss *et al.* 1999), and we are not aware of attempts to isolate the rod-mediated OKR in larval zebrafish. In the present study we have developed a new system for measuring OKR, that allows us to study responses mediated by the rod

pathway. The major changes we employed were as follows. Firstly, the *eclipse* mutation, causing cone degeneration in homozygous larvae (Nishiwaki *et al.* 2008), was bred into the GRK7-transgenic lines to eliminate cone function. Secondly, measurements of OKR were performed on larvae at 21 days post-fertilization (dpf), because rod signalling is not detected until about 15 dpf and is not robust until about 21 dpf in zebrafish larvae according to measurements of the electroretinogram (Bilotta *et al.* 2001). Using these changes we successfully measured rod-mediated OKR from fish with and without GRK7 transgene expression (Fig. 9*A*).

We measured the optokinetic response of larvae under a series of light intensities, from dim to brighter. Representative responses from a 21 dpf GRK7B-tg cone-less larva are illustrated in Fig. 9*A* at two intensities: dim and bright. At the lower light intensity (middle row), the larva exhibited clear OKR: when the drum was rotating either clockwise, CW, or counter-clockwise, CCW, there were smooth tracking movements of the eyes in the direction of the drum rotation, with frequent interruptions by saccades; when the drum was stationary (indicated ZERO) such tracking movements disappeared. At the brighter intensity (bottom row), the eye movements

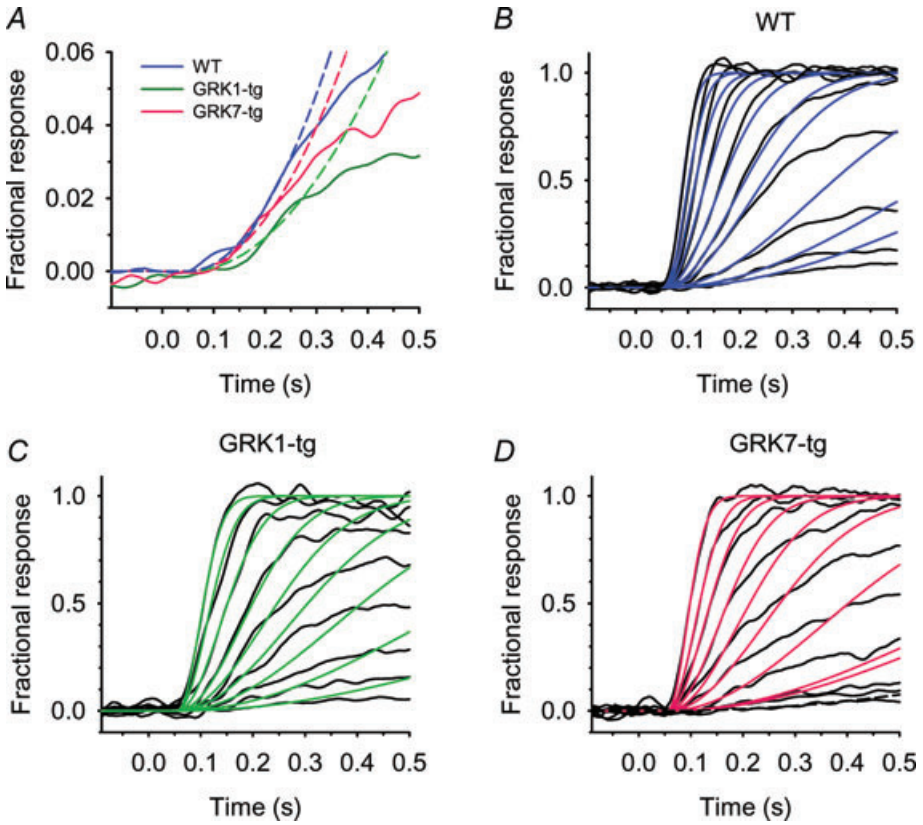

Figure 8. Estimation of the amplification constant (*A*) for representative rods of the three genotypes, from single-photon responses (*A*) and from families of flash responses (*B–D*)
A, onset phase of single-photon response, $a_{var}(t)$, for a representative rod from WT (blue), GRK1-tg (red), and GRK7-tg (green) zebrafish. The parabolas (broken lines) plot the fitted predictions of eqn (6), giving $A = 1.5$, 0.8, and 1.2 s^{-2} respectively. The effective delay time was constrained to $t_{eff} = 48$ ms for each cell, according to the fitting for bright flash responses. For the flash intensities used, these single-photon responses yielded 'functional' effective collecting areas of $A_c = 1.99$, 1.8 and 0.28 μm^2 for the three cells. *B–D*, families of flash responses (black lines) for the three rods in *A*, fitted with the predictions of the Lamb & Pugh model including capacitive time constant (coloured lines; using eqn (5) of Smith & Lamb (1997); the end time for the calculation of fit was varied from 130 ms for bright-flash responses to 250 ms for dim-flash responses. In order to provide an appropriate fit to the responses to brighter flashes, the capacitive time constant was set to 5 ms, and the residual delay of the remaining stages was set to 43 ms, giving a total effective delay time of $t_{eff} = 48$ ms (used above in *A*). The numbers of isomerizations were determined by extrapolation from the intensities that elicited a single photoisomerization according to the a_{var} analysis (which we used above to extract the functional effective collecting area). *B*, WT rod. Flashes delivered from 1.8–900 photoisomerizations for the collecting area of 1.99 μm^2; fitted amplification constant $A = 1.8$ s^{-2}. *C*, GRK1-tg rod. Flashes delivered from 1.7–442 photoisomerizations for the collecting area of 1.8 μm^2; fitted amplification constant $A = 1.0$ s^{-2}. *D*, GRK7-tg rod. Flashes delivered from 1.2–252 photoisomerizations for the collecting area of 0.28 μm^2; fitted amplification constant $A = 1.4$ s^{-2}.

did not appear to correlate with the drum rotation, but instead appeared to be random, and comparable to those when the drum was stationary at the lower intensity. Cone-less fish exhibited detectable OKR over only a restricted range of light intensities. Thus, there was a lower threshold (minimum intensity) below which they did not show OKR, as well as an upper limit (maximum intensity) above which they did not show OKR; the lower threshold showed considerable fish-to-fish variation, whereas the upper limit showed far less variation. Here, we focused on the maximum intensity (upper threshold), which we presume corresponded to the intensity that saturates the rod pathway.

The maximum intensity at which OKR occurred was determined for each fish, and the distributions of the collected results are plotted in the histograms of Fig. 9*B*, for GRK7B-tg fish (red upward bars) and for non-transgenic siblings (blue downward bars), at the two speeds of the drum rotation; all the fish were functionally cone-less. At both speeds of rotation, the maximal intensity for OKR peaked at a log intensity of −2.6 for animals lacking the GRK7 transgene, whereas for animals expressing the transgene the peak was shifted to the right, to a log intensity of −2.0. At the slower speed of rotation (1.5 rpm; left panel), the difference was significant at $P = 0.011$, while at the higher speed of rotation (3 rpm; right panel), the difference was significant at $P = 0.00020$. Similar results were obtained in experiments with another GRK7-tg line, GRK7E (data not shown). These results indicate that, in intact larvae, the light intensities at which the rod pathway

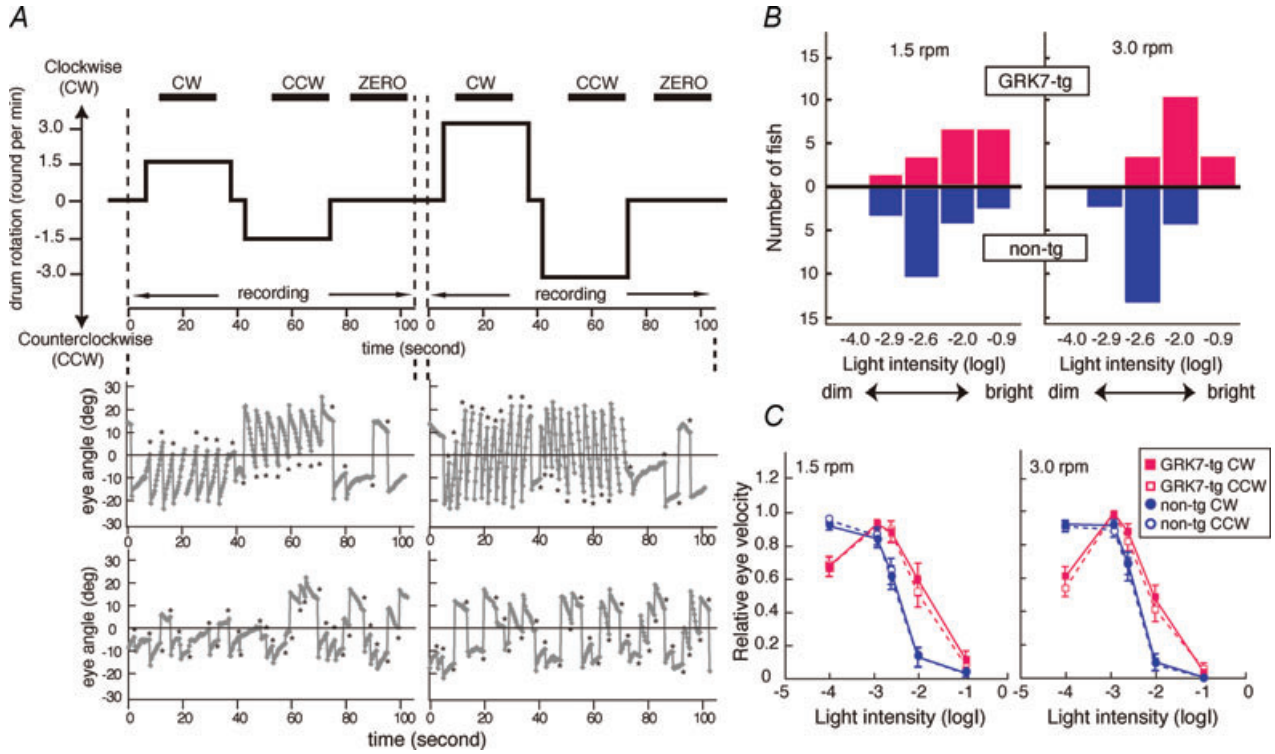

Figure 9. Optokinetic responses for rod-mediated vision of zebrafish larvae deficient in cone function (*els*/*els*)
A, representative measurements of OKR and their analysis. Top, time course of drum rotation. The drum first rotated clockwise (CW) and then counterclockwise (CCW) at 1.5 rpm. After a resting period (ZERO), it rotated at 3 rpm in a similar manner. The horizontal bars at the top indicate the periods used for data processing. Middle and lower panels, representative measurements of eye orientation for two intensities of illumination; −2.0 and −0.9 log units. Middle, at low intensity, the larva showed OKR, consisting of smooth pursuit eye movements followed by rapid saccades (asterisks) in the opposite direction. Bottom, at high intensity, the same larva did not display OKR and the eyes moved apparently at random. *B*, comparison of maximum light intensity to induce OKR for rod-mediated vision in non-transgenic and GRK7-transgenic larvae. In each fish and for each speed, we determined the maximum light intensity at which they showed OKR. The bar graphs plot the distributions of the numbers of fish exhibiting the indicated maximal intensities for eliciting OKR. The distribution for the GRK7-transgenic larvae (red upward bars) was significantly shifted to the right (i.e. to higher intensities) compared with the distribution for non-transgenic larvae (blue downward bars), as statistically examined by Mann–Whitney's *U* test (left, $P = 0.011$; right, $P = 0.00020$). *C*, averaged eye velocity for non-transgenic larvae (blue symbols) and GRK7-tg larvae (red symbols) plotted as a function of light intensity. The direction of rotation is indicated: CW, filled symbols, continuous lines; CCW, open symbols, broken lines. Averages with SEM from 16 GRK7-tg fish and 19 non-transgenic fish are shown.

can operate are higher (possibly by around 4-fold) in animals expressing the GRK7-transgene than in siblings lacking the transgene.

The upward shift in the operational range of the rod pathway in GRK7-tg fish was further supported by a more detailed analysis of eye velocity (Fig. 9*C*). The mean eye velocity of rod-mediated OKR was calculated for each trial and normalized to the highest value (maximum velocity; Supplemental Fig. S5) obtained for each larva over the range of the tested light intensities (see Methods). The normalized eye velocities were plotted as a function of light intensity (Fig. 9*C*). For each speed of OKR stimulation (1.5 or 3 rpm), the intensity–velocity relationship for GRK7B-tg was clearly shifted to higher light intensities (rightward) compared with non-tg controls, as the velocity peaked at log intensities around −3.0 for GRK7-tg and at between −4.0 and −3.0 for non-tg. The shift in the intensity–velocity curve is consistent with the difference in light sensitivity between GRK7-tg and wild-type rods (Fig. 3, and see also Fig. 10 below). It should be noted that the maximum velocity for GRK7-tg animals was as fast as that for non-transgenic controls (Fig. S5). Thus the rod pathways in GRK7-tg and non-transgenic animals may have comparable abilities in discriminating the striped stimuli of the rotating drum, despite the fact that the GRK7-tg rods themselves have slower photoresponse kinetics (Figs 3, 4).

Electrophysiological responses of rods to repetitive steps of light

The stimulus regime in the OKR experiments corresponded to temporal modulation of the illumination at any point on the retina according to a square wave, with a temporal frequency of 0.5 Hz at the faster rotational speed (see Methods). Hence, to investigate the cellular basis for the observed OKR results, we measured the responses of isolated rods, from either WT or GRK7-tg adult zebrafish, to square-wave illumination delivered as 10 cycles of 1 s on and 1 s off, at a range of light intensities. Results from a representative rod of the two genotypes are illustrated in Fig. 10*A* and *B*.

For rods of both genotypes, there was a range of intensities over which the electrical response was substantial, and broadly in-phase with the stimulation. However, as expected for their lower sensitivity, the required intensity range was higher for GRK7-tg rods than for WT rods. For example, at the highest intensity in Fig. 10*A*,*B* (867 photons μm^{-2} s^{-1}, bottom row), the GRK7-tg rod was still responding whereas the WT rod was saturated.

To quantify the mean size of the response to square-wave illumination, we calculated the amplitude of the fundamental component (0.5 Hz) of the response, using Fourier analysis (see Methods). Figure 10*C* shows the amplitude spectrum of the responses obtained for the two cells in Fig. 10*A* and *B*, at the second lowest intensity (14 photons μm^{-2} s^{-1}); as expected the largest component is at 0.5 Hz. For each cell, we normalized the amplitude of the 0.5 Hz component to the largest value obtained at the tested intensities. Then we averaged these normalized amplitudes across cells (6 WT and 6 GRK7-tg rods), and plotted the mean normalized amplitudes as a function of the intensity of the square-wave stimulation in Fig. 10*D*.

There was a clear rightward shift of the response envelope in Fig. 10*D* for the GRK7-tg rods, compared with the WT rods. This shift corresponded to an approximately 4-fold higher intensity in the GRK7-tg rods. Thus, these results provide an explanation for the results of the OKR studies. They indicate that the observed increase in the maximum intensity of white-bar stimulation that evokes OKR responses in cone-less GRK7 transgenic larval zebrafish (compared with WT counterparts) can indeed be explained by the lower sensitivity of their rods.

Discussion

In this study we have investigated the role of GRKs in determining the physiological response properties of photoreceptors, by generating transgenic zebrafish ectopically expressing either GRK7 or GRK1 in their rods, and by then measuring the electrophysiological characteristics of single-cell responses and the behavioural responses of intact animals.

Transgenic zebrafish as a platform for investigation of phototransduction

Our study establishes the zebrafish expression system as a convenient platform for the investigation of specific components of the phototransduction cascade, though the small magnitude of the circulating dark current (~6 pA at room temperature) places constraints on the measurements that can be made. Our single-cell measurements demonstrate that the response properties of WT zebrafish rods are closely similar to those of other vertebrate species, including mammals when allowance is made for the temperature difference.

In recent studies of vertebrate phototransduction, the mouse has become the most commonly used model, because of the availability of gene targeting techniques in this species. Recordings of photoresponses from knockout mice and transgenic mice have revealed the physiological roles of various phototransduction proteins. Another good transgenic platform is *Xenopus*, as the large dimensions of its rods permit analysis of the localisation of proteins.

In comparison with these species, zebrafish provide several advantages for phototransduction studies. Firstly,

in comparison with the very low proportion of cones (~3%) in mouse, the zebrafish retina contains a high proportion of cones (~50%; Wada *et al.* 2006), thereby making the study of cones, and hence of rod/cone differences, more straightforward. Secondly, it is easier and faster to generate stable transgenic lines using zebrafish than most other models. A stable line is greatly preferable to transient transgenesis, to enable precise assessment of

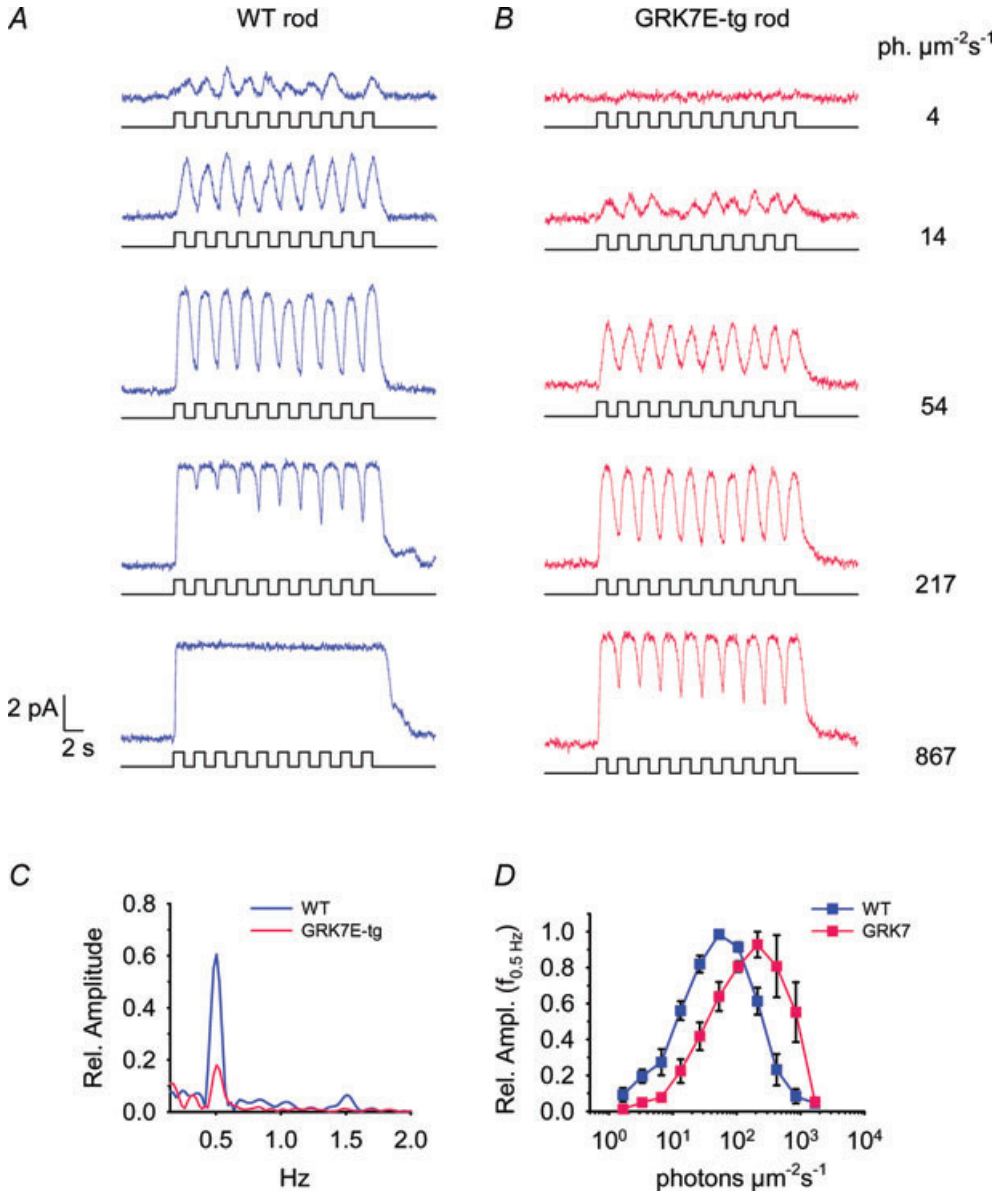

Figure 10. Responses of zebrafish rods to repetitive steps of light at 0.5 Hz
Stimuli consisted of 10 steps of light of 1 s duration, separated by dark periods also of 1 s duration. *A*, responses of a representative WT rod to stimulation at progressively higher intensities. Rectangular traces below each response mark the time course of illumination. At the highest intensity the response remains saturated during the intervals of darkness between the steps of illumination. *B*, responses of a representative GRK7-tg rod to illumination of identical time course and intensity as in *A*. The response is negligible at the lowest intensity, and at the highest intensity the response does not remain in saturation during the dark intervals. *C*, amplitude spectra of the responses at a single intensity (14 photons μm^{-2} s^{-1}), for the traces in *A* and *B*, computed by fast Fourier transform (FFT) analysis. Segments of 20.48 s duration were selected, comprising 4096 points sampled at 200 Hz, beginning at stimulus onset; the amplitudes have been normalized relative to the maximum amplitude of the fundamental (0.5 Hz) component in each rod. Note the smaller relative amplitude of the fundamental component in the GRK7-tg rod (red trace). *D*, averaged amplitude of the fundamental component as a function of light intensity for WT and GRK7-tg rods; results from 3–6 cells have been averaged at each intensity. For GRK7-tg rods the relationship is shifted to the right (to higher intensities).

the effect of transgene expression, particularly when the levels of other phototransduction proteins may be affected by the introduction of the transgene (e.g. as observed in Fig. 1). Moreover, zebrafish are easy and inexpensive to maintain. For single-cell electrophysiology, significant advantages are that the rods of zebrafish are larger than those of mice, and therefore easier to record from, and the recordings can be performed at room temperature rather than at 37°C. For the future, it is likely that the recent progress that has been made in the identification of gene promoters that induce specific expression in rods or cones will further enhance the advantage of zebrafish.

On the other hand, the use of zebrafish has certain limitations. One of the most important is the lack of availability of the homologous recombination technique, which is required for targeted mutagenesis, i.e. production of knock-in animals. However, an alternative method using zinc finger nuclease for targeted gene disruption has recently been developed in zebrafish (Doyon *et al.* 2008; Meng *et al.* 2008; Foley *et al.* 2009). If this could be combined with a reliable method of transgene expression, such as bacterial artificial chromosome (BAC) transgenesis (Yang *et al.* 2006; Suster *et al.* 2009), then this drawback would be overcome. A second limitation is the relatively small size of the circulating dark current, which places constraints on electrophysiological experiments. Finally, although the responses of zebrafish rods appear closely similar to those of other vertebrate species, it is possible that differences from mammalian photoreceptors may be present.

Interpretation of the experiments

Our results show that expression in zebrafish rods of the 'cone-specific' GRK7 (along with the endogenous GRK1) led to a large reduction in sensitivity to light, though not to as low a level as seen in cones. Even though part of this reduction was due to lowered levels of transducin expression (see below), it seems clear that the isoform of GRK expressed in zebrafish photoreceptors (GRK1 in rods and GRK7 in cones) plays a key role in setting the cell's flash sensitivity. In contrast to the effect on sensitivity, the time course of the dim-flash light response in the GRK7-tg transgenic rods was not accelerated (indeed, it was slowed), which was unexpected; below we propose some possible explanations.

Two caveats to our interpretations should be mentioned. Firstly, it is possible that some of the observed differences might be due to the high level of GRK expression in GRK7-tg rods (~5-fold elevation) rather than specifically to the molecular properties of GRK7. Although we cannot rule out this possibility, the fact that GRK7-tg rods retain a sub-class of apparently normal quantal responses suggests that their underlying physiology is little changed. Secondly, we have not been able to take account of possible effects of altered expression levels of other proteins involved in phototransduction. While the levels of rod arrestin, rod guanylate cyclase, recoverin/S-modulin and RGS9 were not significantly changed (Fig. S1), we detected a slight reduction in rhodopsin and a significant reduction in transducin levels (Fig. 1); we could not obtain convincing data on GCAPs, and we do not have information on PDE or other proteins. Hence we cannot rule out confounding effects, such as the possibility that the reduced level of transducin in GRK7-tg rods might contribute in some way to the slowed response kinetics or to a reduced efficacy of activation by R^*.

Possibility of two classes of single-photon response in GRK7-tg rods. Examination of the responses to long series of presentations of extremely dim flashes suggested the existence of two classes of single-photon response in rods of GRK7-tg animals. This led us to hypothesize that the great majority of incident photons trigger small amplitude responses that contribute very little to the response variability, as is observed in cones (Lamb & Simon, 1977), while a small proportion of incident photons trigger larger events exhibiting the conventional quantal properties of rod single-photon responses. For the cell analysed in Fig. 7, the amplitude of the larger event was estimated as $a_L \approx 0.24$ pA. In the same cell, the mean amplitude of the responses composed only of smaller events was $\mu_S = 0.18$ pA at the illustrated intensity of 8 photons μm^{-2}. The calculated 'geometric' effective collecting area for GRK7-tg rods was 2 μm^2 (Table 1), indicating that these flashes would have elicited ~16 isomerizations per flash, the great majority of which are presumed to have triggered small events. Hence the estimated amplitude of the single-photon response underlying the small responses is $a_S \approx 0.012$ pA, around 20-fold smaller than the large quantal events. In fact, the value of 2 μm^2 for the collecting area may be an overestimate (see Results), in which case the actual number of photoisomerizations may have been slightly smaller, and a_S slightly larger.

The difference in amplitude between the larger and smaller events recorded from the rods of GRK7-tg animals is remarkable. This difference demonstrates the profound effect of the sub-type of GRK in determining the sensitivity of the photoreceptor's response to light.

Molecular mechanism for two possible classes of single-photon event. Because of the limited signal-to-noise ratio in the recordings, we cannot be certain that the events do indeed fall neatly into just two categories, of 'small' and 'large'. However, if our preliminary finding is confirmed, then it would seem likely to have an important implication for the molecular mechanism of response shut-off, because it would be consistent with the

hypothesis that the size of the response depends on a single molecular interaction; i.e. on whether the R* binds a GRK7 or a GRK1. In other words, if it is the case that an R* that binds a molecule of GRK7 elicits a small event, whereas an R* that binds a molecule of GRK1 elicits a large event, then the existence of two classes of single-photon event would naturally be expected. We can envisage several scenarios that might lead to a 'first contact' mechanism of this kind.

(1) In a first scenario, suppose that GRK can bind to R* without blocking its access to transducin. Further, suppose that binding of a GRK7 leads to rapid initial phosphorylation, whereas binding of GRK1 leads to a substantial delay before any phosphorylation occurs. And finally, suppose that the mono-phosphorylated state of R* has a substantially lower ability to interact with transducin. In this case, the initial binding of a GRK7 would trigger rapid phosphorylation and thereby reduced activation of transducin, and hence a response of small amplitude; but the initial binding of a GRK1 would lead to a delay in the first phosphorylation, during which time transducin would be activated normally, leading to a response of large amplitude.
(2) In a second scenario, a single molecule of GRK might 'bind and remain', accomplishing the phosphorylation of multiple residues without dissociating to allow access of a different molecule of GRK; in this case the form of the response would again be determined by the identity of the single molecule of GRK that happened to bind.
(3) A third scenario might be that GRK7 and GRK1 preferentially mediate phosphorylation at different residues. If this were the case, then the initial phosphorylation event might provide a 'memory' that would influence subsequent interactions with either GRK7 or GRK1 and thereby potentially lead to two classes of response.

While we have no firm basis for choosing between different models such as these, we simply suggest that there are a number of plausible mechanisms whereby the interaction of a single molecule of GRK could determine the amplitude of the single-photon response.

Possible cellular basis for differences in kinetics. Unexpectedly, the dim-flash response time course was slower in GRK7-tg rods than in WT and GRK1-tg rods. This slowness might be explained either by a specific effect of GRK7 on the shut-off kinetics, or alternatively by some abnormality in the GRK7-tg rods. In the former case, it might for example be possible that GRK7 and GRK1 phosphorylate different residues and that this difference affects the interaction with arrestin. However, we think that the alternative of an indirect effect is more likely. One contributory factor might be the lowered level of GRK1 in GRK7-tg rods (Fig. 1*D*). Another, and perhaps more major contributor, might be some change in the effectiveness of the overall 'cyclase feedback loop', whereby the reduced calcium concentration that accompanies the light response acts via GCAPs to modulate the activity of guanylyl cyclase. Any reduction in the effectiveness of this loop will both slow the recovery of the dim-flash response and increase its amplitude, as occurs for example in GCAPs$^{-/-}$ rods (Burns *et al.* 2002). In fact, the slowing of response recovery in photoreceptors has a powerful effect in increasing the dim-flash response amplitude, with the sensitivity S typically varying with the time-to-peak t_{peak} according to a power law ($S \propto t_{peak}^{n}$) with an exponent of $n \approx 2$–3 (Baylor & Hodgkin, 1974; Baylor *et al.* 1980). Thus an increase in time-to-peak of just 25–40% may typically lead to a doubling of the dim-flash response amplitude.

Activation efficacy. The efficacy of the activation reactions in rods of the three genotypes can be evaluated by comparing the amplification constant (A) of phototransduction (Lamb & Pugh, 1992; Pugh & Lamb, 1993). We obtained $A = 1.5$, 1.1 and 0.9 s^{-2} in WT, GRK1-tg and GRK7-tg rods (Table 1); note that the value for GRK7-tg rods relates to the large events, and the value for the small events would be around 20 times smaller. It is interesting that the ratio of the three values correlates well with the expression levels of transducin in rods of the three genotypes, which were found to be in the ratio of approximately 1:0.9:0.5; thus, the transducin level in GRK7-tg rods was around 50–60% of WT. This correlation is as expected if the amplification constant in rods of the three genotypes is proportional to the transducin level in the outer segments, as has been predicted theoretically (equation (2.2) of Lamb & Pugh (1992)), and observed experimentally in rat rods when transducin migrates as a result of light exposure (Sokolov *et al.* 2002); this is also consistent with the reduced sensitivity in mouse rods heterozygote for transducin knock-out (Calvert *et al.* 2000). These extracted values of amplification constant are also consistent with the observed values of single-photon response amplitude; thus, although GRK7-tg rods had an amplification constant about half that of WT rods, they also exhibited a time-to-peak about 40% longer, which might be expected to roughly double the response amplitude, with the net result that the amplitude of the single-photon response (large events) was similar in GRK7-tg and WT rods.

Macroscopic sensitivity. The difference in measured macroscopic sensitivity between transgenic strains is likely to be a complex matter, determined primarily by (a) the proportion of small *versus* large events, due presumably to shut-off mediated by GRK7 *versus* GRK1, (b) differences in rhodopsin content, (c) sensitivity

differences due to differences in transducin content, and (d) sensitivity differences resulting from differences in response kinetics. We think that the observed ∼8-fold reduction in macroscopic photosensitivity of GRK7-tg rods compared with WT rods is broadly explicable in terms of the combination of these factors. For example, imagine a hypothetical GRK7-tg rod, in which (a) 10% of R*s are shut-off via GRK1 while the remaining 90% are shut-off via GRK7 giving 20-fold smaller responses, and (b) with 80% of the rhodopsin content of WT, (c) 50% of the transducin content, and (d) dim-flash responses twice as large due to the slower kinetics. In this case, the expected sensitivity would be roughly $(0.1 + 0.9 \times 1/20) \times 0.8 \times 0.5 \times 2 = 0.12$, corresponding to slightly more than an 8-fold increase in half-saturating intensity, $Q_{1/2}$. While the numbers used in this calculation are only rough estimates, the exercise indicates that the measured macroscopic sensitivity appears to fit broadly with our expectations.

Dominant time constant. Although the rods of GRK7-tg animals exhibited slower dim-flash responses than in WT ($t_{peak} \approx 0.84$ s *cf* 0.57 s), the dominant time constant for the recovery from bright flashes did not appear different, at least for intensities up to 10^4 photons μm^{-2} or around 20 000 photoisomerizations per flash (e.g. $\tau_{dom,\,med} \approx 0.95$ s for both; see Fig. 3*E* and Table 1). The most parsimonious explanation for the unaltered kinetics of bright flash recovery is that, just as in mouse rods (Krispel *et al.* 2006), the dominant time constant of recovery in zebrafish rods is determined not by rhodopsin phosphorylation, but instead by the shut-off of the activated transducin/PDE complex, accelerated by RGS9. If this is the case, then it would indicate that the lifetime of activated transducin is normal. In support of this notion, we found that the expression levels of the proteins that we could measure (rod arrestin, rod guanylate cyclase, recoverin/S-modulin and RGS9) were comparable among the three genotypes (Fig. 1*G* and Fig. S1), and we have no reason to think that the level of PDE was altered.

OKR. Our experiments on intact animals conformed to the expectations reported above for single-cell recordings. Thus in GRK7-tg animals, the light intensity required to initiate optokinetic responses was higher than in WT animals and likewise the uppermost intensity at which OKR was elicited in cone-less animals was higher in GRK7-tg animals than in WT. We interpret this uppermost intensity for OKR in cone-less animals to reflect the intensity needed to saturate the rod pathway. To support this interpretation we conducted single-cell experiments using a comparable square-wave time course of illumination, and found that saturation of the rods themselves occurred at a higher intensity in GRK7-tg rods than in WT rods. We presume that the elevated saturating intensity in GRK7-tg is caused by the substantially lower flash sensitivity, and is somewhat counteracted by the slower kinetics of the recovery of the light responses.

In conclusion, expression of exogenous GRK7 in zebrafish rods (in addition to the endogenous GRK1) leads to lowered flash sensitivity. Each photoisomerized rhodopsin molecule elicits either a relatively normal (rod-like) quantal response or else a greatly attenuated (cone-like) response, and we propose that this dichotomy results from whether the R* interacts with a single molecule of GRK1 or of GRK7. Both the larger and the smaller quantal responses are slower than in WT rods, for several possible reasons that we offer above. As in mouse rods, the shut-off of R* is faster than the shut-off of transducin/PDE, so that expression of GRK7 reduces response sensitivity without accelerating response kinetics. The transgenic zebrafish model is likely to be a powerful platform for further investigation of the molecular basis of photoreceptor responses.

References

Arinobu D, Tachibanaki S & Kawamura S (2010). Larger inhibition of visual pigment kinase in cones than in rods. *J Neurochem* **115**, 259–268.

Asaoka Y, Mano H, Kojima D & Fukada Y (2002). Pineal expression-promoting element (PIPE), a cis-acting element, directs pineal-specific gene expression in zebrafish. *Proc Natl Acad Sci U S A* **99**, 15456–15461.

Baylor DA & Hodgkin AL (1974). Changes in time scale and sensitivity in turtle photoreceptors. *J Physiol* **242**, 729–758.

Baylor DA, Hodgkin AL & Lamb TD (1974). The electrical response of turtle cones to flashes and steps of light. *J Physiol* **242**, 685–727.

Baylor DA, Lamb TD & Yau KW (1979*a*). The membrane current of single rod outer segments. *J Physiol* **288**, 589–611.

Baylor DA, Lamb TD & Yau KW (1979*b*). Responses of retinal rods to single photons. *J Physiol* **288**, 613–634.

Baylor DA, Matthews G & Yau KW (1980). Two components of electrical dark noise in toad retinal rod outer segments. *J Physiol* **309**, 591–621.

Baylor DA, Matthews G & Yau KW (1983). Temperature effects on the membrane current of retinal rods of the toad. *J Physiol* **337**, 723–734.

Bilotta J, Saszik S & Sutherland SE (2001). Rod contributions to the electroretinogram of the dark-adapted developing zebrafish. *Devel Dyn* **222**, 564–570.

Bradford MM (1976). A rapid and sensitive method for the quantitation of microgram quantities of protein utilizing the principle of protein-dye binding. *Anal Biochem* **72**, 248–254.

Brockerhoff SE, Hurley JB, Janssen-Bienhold U, Neuhauss SC, Driever W & Dowling JE (1995). A behavioral screen for isolating zebrafish mutants with visual system defects. *Proc Natl Acad Sci U S A* **92**, 10545–10549.

Burns ME, Mendez A, Chen J & Baylor DA (2002). Dynamics of cyclic GMP synthesis in retinal rods. *Neuron* **36**, 81–91.

Calvert PD, Krasnoperova NV, Lyubarsky AL, Isayama T, Nicolo M, Kosaras B, Wong G, Gannon KS, Margolskee RF, Sidman RL, Pugh EN Jr, Makino CL & Lem J (2000). Phototransduction in transgenic mice after targeted deletion of the rod transducin α-subunit. *Proc Natl Acad Sci U S A* **97**, 13913–13918.

Doyon Y, McCammon JM, Miller JC, Faraji F, Ngo C, Katibah GE, Amora R, Hocking TD, Zhang L, Rebar EJ, Gregory PD, Urnov FD & Amacher SL (2008). Heritable targeted gene disruption in zebrafish using designed zinc-finger nucleases. *Nat Biotechnol* **26**, 702–708.

Foley JE, Yeh JR, Maeder ML, Reyon D, Sander JD, Peterson RT & Joung JK (2009). Rapid mutation of endogenous zebrafish genes using zinc finger nucleases made by Oligomerized Pool ENgineering (OPEN). *PLoS One* **4**, e4348.

Fu Y & Yau KW (2007). Phototransduction in mouse rods and cones. *Pflugers Arch* **454**, 805–819.

Hamer RD, Nicholas SC, Tranchina D, Liebman PA & Lamb TD (2003). Multiple steps of phosphorylation of activated rhodopsin can account for the reproducibility of vertebrate rod single-photon responses. *J Gen Physiol* **122**, 419–444.

Hisatomi O, Matsuda S, Satoh T, Kotaka S, Imanishi Y & Tokunaga F (1998). A novel subtype of G-protein-coupled receptor kinase, GRK7, in teleost cone photoreceptors. *FEBS Lett* **424**, 159–164.

Hisatomi O & Tokunaga F (2002). Molecular evolution of proteins involved in vertebrate phototransduction. *Comp Biochem Physiol B* **133**, 509–522.

Hurley JB (1992). Signal transduction enzymes of vertebrate photoreceptors. *J Bioenerg Biomembr* **24**, 219–226.

Jarvinen JLP & Lamb TD (2005). Inverted photocurrent responses from amphibian rod photoreceptors: Role of membrane voltage in response recovery. *J Physiol* **566**, 455–466.

Kawakami K, Takeda H, Kawakami N, Kobayashi M, Matsuda N & Mishina M (2004). A transposon-mediated gene trap approach identifies developmentally regulated genes in zebrafish. *Devel Cell* **7**, 133–144.

Kawamura S & Tachibanaki S (2008). Rod and cone photoreceptors: Molecular basis of the difference in their physiology. *Comp Biochem Phys A* **150**, 369–377.

Koskelainen A, Donner K, Kalamkarov G & Hemila S (1994). Changes in the light-sensitive current of salamander rods upon manipulation of putative pH-regulating mechanisms in the inner and outer segment. *Vision Res* **34**, 983–994.

Krispel CM, Chen D, Melling N, Chen YJ, Martemyanov KA, Quillinan N, Arshavsky VY, Wensel TG, Chen CK & Burns ME (2006). RGS expression rate-limits recovery of rod photoresponses. *Neuron* **51**, 409–416.

Lamb TD (1984). Effects of temperature changes on toad rod photocurrents. *J Physiol* **346**, 557–578.

Lamb TD, Matthews HR & Torre V (1986). Incorporation of calcium buffers into salamander retinal rods: a rejection of the calcium hypothesis of phototransduction. *J Physiol* **372**, 315–349.

Lamb TD, McNaughton PA & Yau KW (1981). Spatial spread of activation and background desensitization in toad rod outer segments. *J Physiol* **319**, 463–496.

Lamb TD & Pugh EN Jr (1992). A quantitative account of the activation steps involved in phototransduction in amphibian photoreceptors. *J Physiol* **449**, 719–758.

Lamb TD & Simon EJ (1977). Analysis of electrical noise in turtle cones. *J Physiol* **272**, 435–468.

Maeda T, Imanishi Y & Palczewski K (2003). Rhodopsin phosphorylation: 30 years later. *Prog Retinal Eye Res* **22**, 417–434.

Meng X, Noyes MB, Zhu LJ, Lawson ND & Wolfe SA (2008). Targeted gene inactivation in zebrafish using engineered zinc-finger nucleases. *Nat Biotechnol* **26**, 695–701.

Murnick JG & Lamb TD (1996). Kinetics of desensitization induced by saturating flashes in toad and salamander rods. *J Physiol* **495**, 1–13.

Neuhauss SC, Biehlmaier O, Seeliger MW, Das T, Kohler K, Harris WA & Baier H (1999). Genetic disorders of vision revealed by a behavioral screen of 400 essential loci in zebrafish. *J Neurosci* **19**, 8603–8615.

Nishiwaki Y, Komori A, Sagara H, Suzuki E, Manabe T, Hosoya T, Nojima Y, Wada H, Tanaka H, Okamoto H & Masai I (2008). Mutation of cGMP phosphodiesterase 6 α-subunit gene causes progressive degeneration of cone photoreceptors in zebrafish. *Mechanisms Devel* **125**, 932–946.

Nymark S, Heikkinen H, Haldin C, Donner K & Koskelainen A (2005). Light responses and light adaptation in rat retinal rods at different temperatures. *J Physiol* **567**, 923–938.

Pepperberg DR, Cornwall MC, Kahlert M, Hofmann KP, Jin J, Jones GJ & Ripps H (1992). Light-dependent delay in the falling phase of the retinal rod photoresponse. *Vis Neurosci* **8**, 9–18.

Pugh EN Jr & Lamb TD (1993). Amplification and kinetics of the activation steps in phototransduction. *Biochim Biophys Acta* **1141**, 111–149.

Rieke F & Baylor DA (1998). Origin of reproducibility in the responses of retinal rods to single photons. *Biophys J* **75**, 1836–1857.

Rinner O, Makhankov YV, Biehlmaier O & Neuhauss SC (2005). Knockdown of cone-specific kinase GRK7 in larval zebrafish leads to impaired cone response recovery and delayed dark adaptation. *Neuron* **47**, 231–242.

Robinson DW, Ratto GM, Lagnado L & McNaughton PA (1993). Temperature dependence of the light response in rat rods. *J Physiol* **462**, 465–481.

Smith NP & Lamb TD (1997). The a-wave of the human electroretinogram recorded with a minimally invasive technique. *Vision Res* **37**, 2943–2952.

Sokolov M, Lyubarsky AL, Strissel KJ, Savchenko AB, Govardovskii VI, Pugh EN Jr & Arshavsky VY (2002). Massive light-driven translocation of transducin between the two major compartments of rod cells: a novel mechanism of light adaptation. *Neuron* **34**, 95–106.

Suster ML, Sumiyama K & Kawakami K (2009). Transposon-mediated BAC transgenesis in zebrafish and mice. *BMC Genomics* **10**, 477.

Tachibanaki S, Arinobu D, Shimauchi-Matsukawa Y, Tsushima S & Kawamura S (2005). Highly effective phosphorylation by G protein-coupled receptor kinase 7 of light-activated visual pigment in cones. *Proc Natl Acad Sci U S A* **102**, 9329–9334.

Tachibanaki S, Tsushima S & Kawamura S (2001). Low amplification and fast visual pigment phosphorylation as mechanisms characterizing cone photoresponses. *Proc Natl Acad Sci U S A* **98**, 14044–14049.

Takemoto N, Tachibanaki S & Kawamura S (2009). High cGMP synthetic activity in carp cones. *Proc Natl Acad Sci U S A* **106**, 11788–11793.

Urasaki A, Morvan G & Kawakami K (2006). Functional dissection of the Tol2 transposable element identified the minimal cis-sequence and a highly repetitive sequence in the subterminal region essential for transposition. *Genetics* **174**, 639–649.

Wada Y, Sugiyama J, Okano T & Fukada Y (2006). GRK1 and GRK7: unique cellular distribution and widely different activities of opsin phosphorylation in the zebrafish rods and cones. *J Neurochem* **98**, 824–837.

Wald G & Brown PK (1953). The molar extinction coefficient of rhodopsin. *J Gen Physiol* **37**, 189–200.

Whitlock GG & Lamb TD (1999). Variability in the time course of single photon responses from toad rods: termination of rhodopsin's activity. *Neuron* **23**, 337–351.

Yang Z, Jiang H, Chachainasakul T, Gong S, Yang XW, Heintz N & Lin S (2006). Modified bacterial artificial chromosomes for zebrafish transgenesis. *Methods* **39**, 183–188.

Zhao X, Huang J, Khani SC & Palczewski K (1998). Molecular forms of human rhodopsin kinase (GRK1). *J Biol Chem* **273**, 5124–5131.

Author contributions

Y.F., S.K. and T.D.L. conceived and designed the research. Y.W., J.S. and K.K. generated transgene constructs. Y.W. and J.S. generated transgenic zebrafish. Y.W. performed immunohistochemistry. T.S. performed spectrophotometry, immunoblot analysis and phosphorylation assays. F.V. and J.L.P.J. performed single-cell electrophysiological recordings. F.V. and T.D.L. analysed electrophysiological data. T.S., D.K., Y.W., Y.N. and I.M. performed optokinetic response measurements. F.V., T.D.L., T.S., D.K. and Y.F. wrote the manuscript. All authors approved the manuscript for publication. Electrophysiological experiments were conducted in the Department of Neuroscience, John Curtin School of Medical Research, ANU, Australia. Optokinetic response measurements were conducted in Department of Biophysics and Biochemistry, Graduate School of Science, University of Tokyo, and Developmental Neurobiology Unit, OIST, Okinawa, Japan. All other experiments were conducted in the Department of Biophysics and Biochemistry, Graduate School of Science, University of Tokyo, Japan.

Acknowledgements

We thank Junko Tomizuka (Osaka University) for allowing us to use the unpublished antibody (anti-carp Arr1). This research was supported in part by the Human Frontier Science Program (to S.K., Y.F. and T.D.L.), by the Australian Research Council through the ARC Centre of Excellence in Vision Science (CE0561903) to T.D.L., by Grants-in-Aid for scientific research from MEXT, Japan (to D.K., K.S. and Y.F.) and by Global COE Program (Integrative Life Science Based on the Study of Biosignaling Mechanisms) from MEXT, Japan. T.S. is a Research Fellow of the Japan Society for the Promotion of Science.